MEASUREMENT OF THRUST & PROPULSIVE EFFICIENCY OF FLEXIBLE FOIL PERFORMING HEAVE MOTION

A thesis
submitted in partial fulfilment of the
requirement for the degree of

Master of Technology
In
MECHANICAL ENGINEERING

Submitted By
Shubham Agrawal

Under the Guidance of
Prof. Raghuraman N. Govardhan

Department of Mechanical Engineering
Indian Institute of Science
Bangalore-560012, India

Acknowledgements

I am very glad to have this opportunity to express my sincere gratitude to everyone who assisted me in different ways. Firstly, I am very grateful to my research advisor Prof. Raghuraman N. Govardhan for his continuous guidance and encouragement. I would like to thank him for motivating me to face challenges in my research.

I attended numerous courses offered by the eminent professors of our department. I want to convey my sincere gratitude to all the instructors for their untiring efforts which helped me to understand my research domain thoroughly. I would like to thank Prof. Venkata R. Sonti and Dr. Ratnesh K. Shukla for reviewing my work and for their valuable feedback.

I would like to thank office staff especially Mrs. Somavati & Ms. Chinnamma for their guidance in official matters, which helped in smooth progression of my course work.

I gratefully acknowledge the assistance and guidance of my lab mates. The research environment and the insightful discussions in the lab motivated me a lot during my research work. I thank all my batch mates for their support and making my life at IISc such pleasurable. Finally, I want to thank my parents and my brother for their inseparable support throughout the duration of my studies. I dedicate my thesis to my parents.

Shubham

Abstract

Increase in the use of autonomous underwater vehicles has enhanced interest in the study of their propulsive performance, namely, their thrust and efficiency. The highly efficient swimming mechanisms of fish can potentially provide inspiration for the design of propulsors that will outperform the propeller-based thrusters currently in use. In the present work, the thrust generation and the propulsive efficiency of a flexible heaving foil has been studied experimentally. The flexible foil comprises of a rigid NACA 0012 foil (chord length, c) with a flexible flap of length C_f, and flexural rigidity EI attached to its trailing edge. We have investigated thrust generation for a range of flexural rigidities, EI, keeping flap length to total chord ratio, $\frac{C_F}{C} = 0.45$, constant. Flexural rigidity is non-dimensionalized as $R^{*}=\frac{EI}{0.5\rho u^2 {C_f}^3}$. Thrust generation in pure heave oscillation is purely due to axial force and power required is directly proportional to the normal component of force. Experiments have been performed for two values of heave amplitude to chord ratio (h_0/c) i.e. 0.11 and 0.32. Thrust coefficient (C_T), power coefficient (C_P), and the propulsive efficiency (η) are determined as a function of Strouhal number (St) and the non-dimensional flexural rigidity R* at both the heaving amplitudes. The overall maximum efficiency obtained is 35.2 % for h_0/c = 0.11 at St = 0.16 and R* = 0.473, but the corresponding C_T is 0.167 which is significantly low. For the larger heave amplitude case of h_0/c = 0.32, the maximum efficiency attained is 25.43 % at St = 0.3 for rigid foil with corresponding C_T = 0.51. These values of efficiency may be compared with the corresponding rigid foil cases.

Notations

[C_M] =Magnitude of non-dimensional moment coefficient

[C_N]= Magnitude of non-dimensional normal force coefficient

[C_A]= Magnitude of non-dimensional axial force coefficient

C *=Total chord length of the foil*

ω= Angular frequency,ω=$2\pi f$

k*= Reduced frequency or normalized frequency,*$k = \pi f c/u$

u *=Mean free stream velocity of water in tunnel*

C_T*= Mean total thrust coefficient*

C_P*=Mean total power coefficient*

C_{TA}*= Mean axial thrust coefficient*

C_{TN}*= Mean normal thrust coefficient*

η *=Efficiency,*$\eta = \frac{\overline{C_T}}{\overline{C_P}}$

f*= Frequency of pitching oscillation*

F_A*=Force parallel to the chord*

F_N*=Force normal to the chord*

Re*=Reynolds number,*$Re = \rho uc/\mu$*,ρ is water density and μ is dynamic viscocity*

s *=Maximum span of the foil*

C_R *=Rigid chord length*

C_F *= Flexible chord length*

θ*= Instantaneous angle of the foil*

θ_0 *=Maximum angle of oscillation*

R^* = Non-dimensional stiffness parameter, $R^* = EI/(0.5\rho u^2 s c_F^3)$

St=Strouhal number =fA/u, f is frequency of oscillation, A is rigid tip to tip maximum excursion

Index

List of figures

1 Introduction

Fish swim in a variety of different ways. This includes wavelike movements of the fish's body and tail, and in others by movements of the fins. Fish swim by exerting force against the surrounding water. The vector forces exerted on the water by such motion cancel out laterally in the mean but generate a net force backwards which in turn pushes the fish forward through the water. Most fishes generate thrust using lateral movements of their body and caudal fin, but many other species move mainly using their median and paired fins (Figure 1.1).

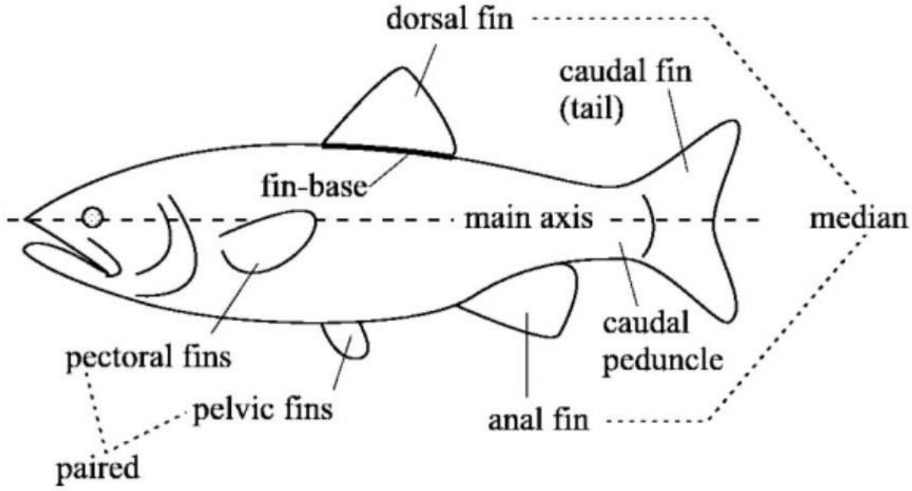

Figure 1. 3: Modes of fish Swimming (Lindsey (1978)) [8].

1.1 Forces acting on a swimming fish

The main properties of water as a locomotion medium that have played an important role in the evolution of fish are its incompressibility and its high density. Since water is an incompressible fluid, any movement executed by an aquatic animal will set the water surrounding it in motion and vice versa. Its density (about 800 times that of air) is sufficiently close to that of the body of marine animals to nearly counterbalance the force of gravity. This has allowed the development of a great variety of swimming propulsors, as weight support is not of primary importance. Swimming of fishes involves the transfer of momentum from the fish to the surrounding water (and vice versa). The main momentum transfer mechanisms are via drag, lift, and acceleration reaction forces. Swimming drag consists of the following components:

1) skin friction between the fish and the boundary layer of water (viscous or friction drag): Friction drag arises as a result of the viscosity of water in areas of flow with large velocity gradients.
2) pressures formed in pushing water aside for the fish to pass (form drag). Form drag is caused by the distortion of flow around solid bodies and depends on their shape.
3) energy lost in the vortices formed by the caudal and pectoral fins as they generate lift or thrust (vortex or induced drag): Induced drag depends largely on the shape of these fins.

The forces acting on a swimming fish are weight, buoyancy, and hydrodynamic lift in the vertical direction, along with thrust and resistance in the horizontal direction (See figure 1.2).

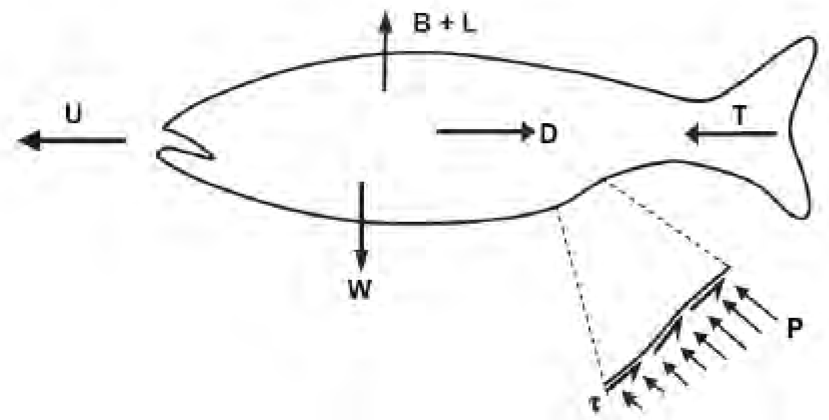

Figure 1. 4 : Schematic showing forces acting on a fish at constant speed (Journal of the Indian Institute of Science VOL 91:3 July–Sept. 2011) [7].

For a fish propelling itself at a constant speed, the momentum conservation principle requires that the forces and moments acting on it are balanced. Therefore, the total thrust it exerts against the water must be equal to the total resistance it encounters moving forward. Pressure drag, lift, and acceleration reaction can all contribute to both thrust and resistance. However, since lift generation is associated with the intentional movement of propulsors by fish, it only contributes to resistance for actions such as braking and stabilization rather than for steady swimming. Additionally, viscous drag always contributes to resistance forces. Finally, body inertia, although not a momentum transfer mechanism, contributes to the water resistance as it opposes acceleration from rest and tends to maintain motion once begun. The main factors determining the relative contributions of the momentum transfer mechanisms to thrust and resistance are:

1) Reynolds number (Re);
2) reduced frequency (k);
3) and shape

The Reynolds number Re is the ratio of inertial over viscous forces, defined as

$$Re = \rho uc/\mu$$

Where, ρ denotes the fluid density; u denotes the velocity of fish; c denotes chord length and μ denotes dynamic viscosity.

In the realm of Re typical of adult fish swimming (i.e.$10^3 < < 5*10^6$), inertial forces are dominant and viscous forces are usually neglected. At those Re, acceleration reaction, pressure drag, and lift mechanisms can all generate effective forces.

The reduced frequency k indicates the importance of unsteady (time-dependent) effects in the flow and is defined as

$$k=\pi f c/u$$

The reduced frequency essentially compares the time taken for a particle of water to traverse the length of an object with the time taken to complete one movement cycle. It is used as a measure of the relative importance of acceleration reaction to pressure drag and lift forces. Finally, the shape of the swimming fish and the specific propulsor utilized largely affect the magnitude of the force components. Strouhal number is another important dimensionless term, given by

$$St=fA/u$$

Where, A denotes twice the amplitude of trailing edge.

1.2 Thrust production in fishes

Most fish generate thrust by bending their bodies into a backward-moving propulsive wave that extends to its caudal fin, a type of swimming classified under body and/or caudal fin (BCF) locomotion. Other fish have developed alternative swimming mechanisms that involve the use of their median and pectoral fins, termed median and/or paired fin (MPF) locomotion. An estimated 15% of the fish families use non-BCF modes as their routine propulsive means, while a much greater number that typically rely on BCF modes for propulsion employ MPF modes for maneuvering and stabilization. In undulatory BCF modes, the propulsive wave traverses the fish body in a direction opposite to the overall movement and at a speed greater than the overall swimming speed.

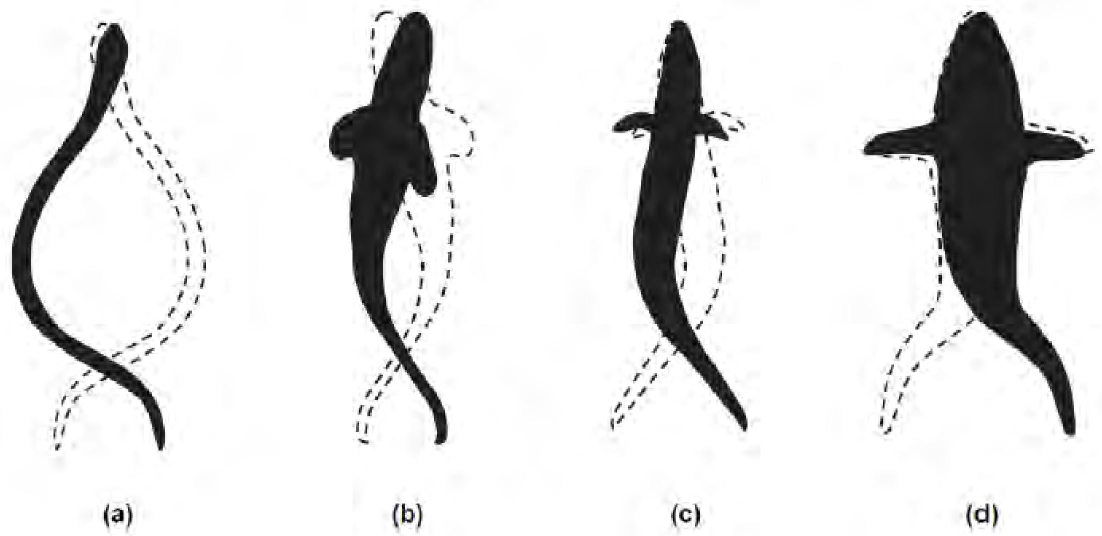

Figure 1. 5: Different fish swimming modes going from nearly whole body undulatory motion in (a) to predominantly caudal tail oscillatory motion in (d). (a) Anguilliform (e.g. eel), (b) Sub-carangiform (e.g. trout), (c) Carangiform (e.g. bluefish), and (d) Thunniform (e.g. sharks). Figure is adapted from Lindsey (1978) [8].

The four undulatory BCF locomotion modes in fish (Figure 1.3) are anguilliform, in which a wave passes evenly along a long slender body; sub-carangiform, in which the wave increases quickly in amplitude towards the tail; carangiform, in which the wave is concentrated near the tail, which oscillates rapidly; thunniform, rapid swimming with a large powerful crescent-shaped tail; and ostraciiform, with almost no oscillation except of the tail fin. More specialized fish include movement by pectoral fins with a mainly stiff body, as in the sunfish; and movement by propagating a wave along the long fins with a motionless body in fish with electric organs such as the knifefish.

In Figure 1.4 the wake downstream of (a) the drag producing fish body, (b) thrust producing flapping tail (or propeller) and (c) the sum of the drag producing body and the thrust producing tail. In the case of a fish in steady forward motion (as in (c)), the net momentum in the wake is zero, as the drag on the body is balanced by the thrust from the tail. In all cases, the body is moving to the left through stationary fluid. The viscous boundary layer on the fish body is shown by the shaded dark region.

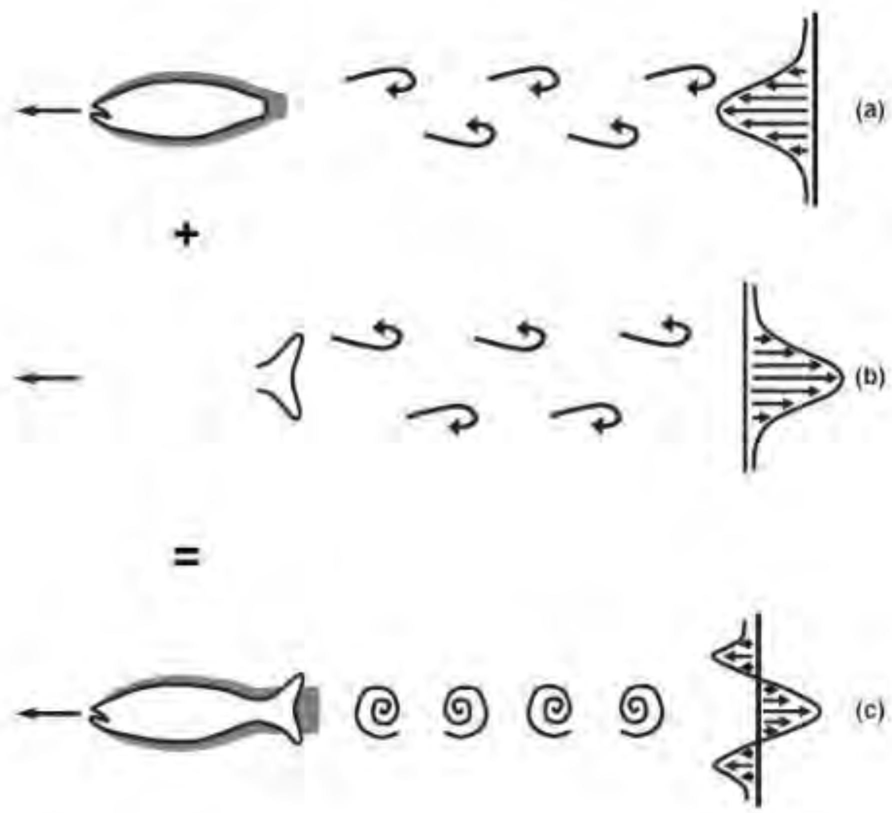

Figure 1. 6: Showing the wake downstream of (a) the drag producing fish body, (b) thrust producing flapping tail (or propeller) and (c) the sum of the drag producing body and the thrust producing tail (Journal of the Indian Institute of Science VOL 91:3 July–Sept. 2011) [7].

With recent advent of Digital Particle Image Velocimetry (PIV), researchers are able to capture velocity fields around fishes. However, the wakes of fishes are 3-dimensional, and one can't directly measure forces on a fish (say using a load cell) and its difficult to train and control fishes. So, it is useful to first understand an equivalent system involving unsteady motion of a foil. Fishes in the Ostraciiform category use only the tail to generate thrust, and though the tail is 3-dimensional, one can consider its cross-section as a thin foil. The motion of a fish is inherently unsteady even when it is swimming 'steadily'. Flapping involves periodic motion of the tail, and periodic motions involve both angular acceleration and deceleration, hence bringing in the unsteadiness. The drag and lift forces due to such unsteady flows is not as well understood as for steady motions.

1.3 Literature review

The interest in the field of flapping airfoil goes back to 20th century. Garrick (1936) provided the expressions for the mean Thrust produced by an oscillating airfoil and the mean Power input oscillating in any of the three degrees of freedom: vertical flapping, torsional oscillations about a fixed axis parallel to the span, and angular oscillations of the airfoil about a hinge. Delaurier and Harris (1982), have done experiments on oscillating wing propulsion with combined heave and pitch and found that thrust produced is linearly dependent on the reduced frequency and best performance is obtained when pitching is lagging heaving by phase angle of 90-120 degrees. Freymuth (1988) studied the vortical generation by airfoils performing pure plunging and pure pitching motion. M. S. Triantafyllou et al. (1998) did a set of experiments with combined heaving and pitching oscillation in which they played with the heave amplitude to chord ratio, strouhal number, angle of attack and phase difference between heaving and pitching oscillation. The highest recorded efficiency in these experiments (Figure 1.5) for high thrust production (Figure 1.6) was equal to 87%, and was obtained for amplitude to chord ratio ho/c = 0.75, angle of attack α_{max} = 20.2^0, phase angle = 75^0; and at approximately Strouhal Number St_{TE} = 0.36

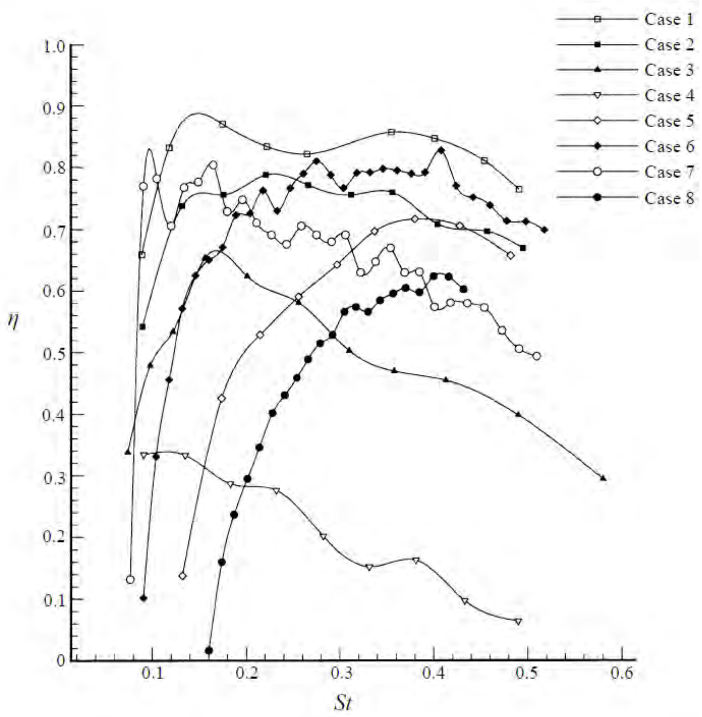

Figure 1. 7: Experimentally measured efficiency as function of the Strouhal number St_{TE}. Curve 1 : h_0/c = 0.75, α_{max} = 21^0, φ = 75^0; Curve 2 : h_0/c = 0.75, α_{max} = 17^0, φ = 105^0; Curve 3 : h_0/c = 0.25, α_{max} = 15^0, φ = 90^0; Curve 4 : h_0/c = 0.75, α_{max} = 5^0, φ = 90^0; Curve 5 : h_0/c = 0.75, α_{max} = 25^0, φ = 90^0; Curve 6 : h_0/c = 0.75, α_{max} = 20^0, φ = 90^0; Curve 7 : h_0/c = 0.75, α_{max} = 10^0, φ = 90^0; Curve 8 : h_0/c = 0.75, α_{max} = 30^0, φ = 90^0. Figure is adapted from Triantafyllou (1998) [5]

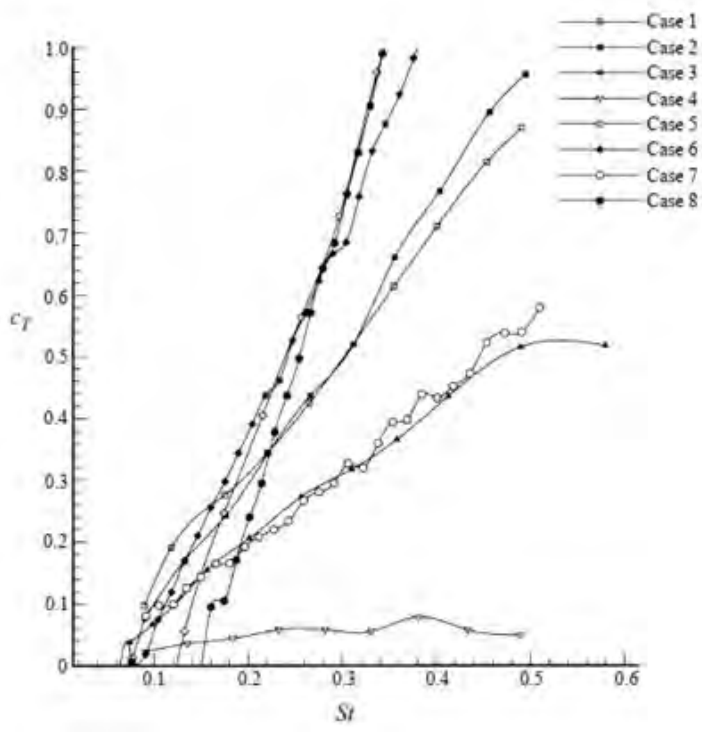

Figure 1. 8: Experimentally measured thrust coefficient C_T as a function of strouhal number $S_{TE.}$ Curve 1 : $h_0/c = 0.75$, $\alpha_{max} = 21^0$, $\varphi = 75^0$; Curve 2 : $h_0/c = 0.75$, $\alpha_{max} = 17^0$, $\varphi = 105^0$; Curve 3 : $h_0/c = 0.25$, $\alpha_{max} = 15^0$, $\varphi = 90^0$; Curve 4 : $h_0/c = 0.75$, $\alpha_{max} = 5^0$, $\varphi = 90^0$; Curve 5 : $h_0/c = 0.75$, $\alpha_{max} = 25^0$, $\varphi = 90^0$; Curve 6 : $h_0/c = 0.75$, $\alpha_{max} = 20^0$, $\varphi = 90^0$; Curve 7 : $h_0/c = 0.75$, $\alpha_{max} = 10^0$, $\varphi = 90^0$; Curve 8 : $h_0/c = 0.75$, $\alpha_{max} = 30^0$, $\varphi = 90^0$. Figure is adapted from Triantafyllou (1998) [5]

Triantafyllou et al. (2003) studied the airfoil performing combined heaving and pitching oscillation and obtained Thrust Coefficient as high as 2.4 (Figure 1.7) for 35° maximum angle of attack and phase angle between heave and pitch as 100^0

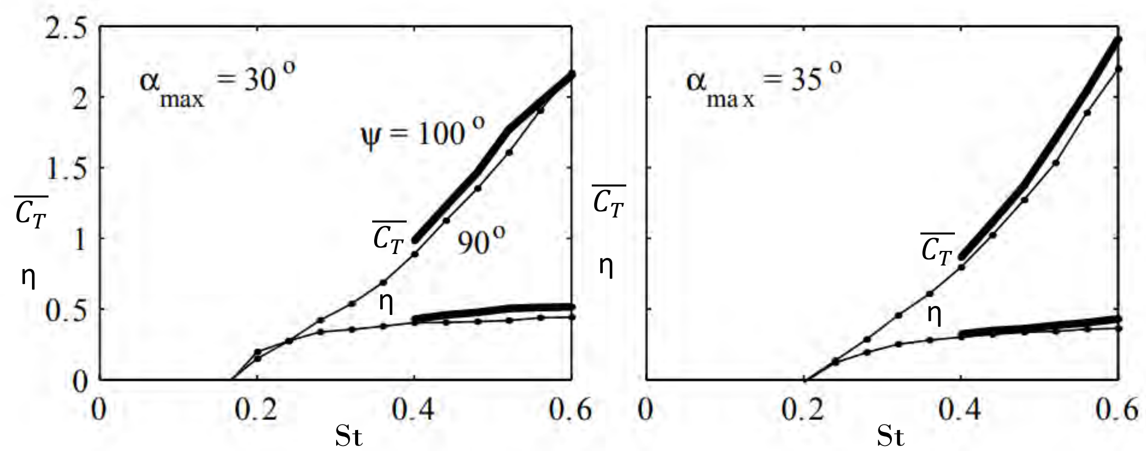

Figure 1. 9: Variation of Thrust Coefficient with Strouhal Number for maximum angle of attack 30^0 and 35^0 with phase angle of 90^0 and 100^0. Figure is adapted from Triantafyllou (2003) [6]

J. M. Miao and M. H. Ho (2006) have studied numerically the effect of flexure on aerodynamic propulsive efficiency of flapping flexible airfoil. They found that the peak propulsive efficiency obtained at constant Reynolds numbers of 10^2, 10^3 and 10^4 occurs at reduced frequencies of 5, 3 and 2, respectively (Figure 2.4). Of the various runs performed in the present study, the airfoil with maximum heave amplitude to chord ratio of 0.3 moving under conditions of Re = 10^4 and k = 2, corresponding to a Strouhal number of approximately 0.255, demonstrates the highest propulsive efficiency, namely 30.73%.

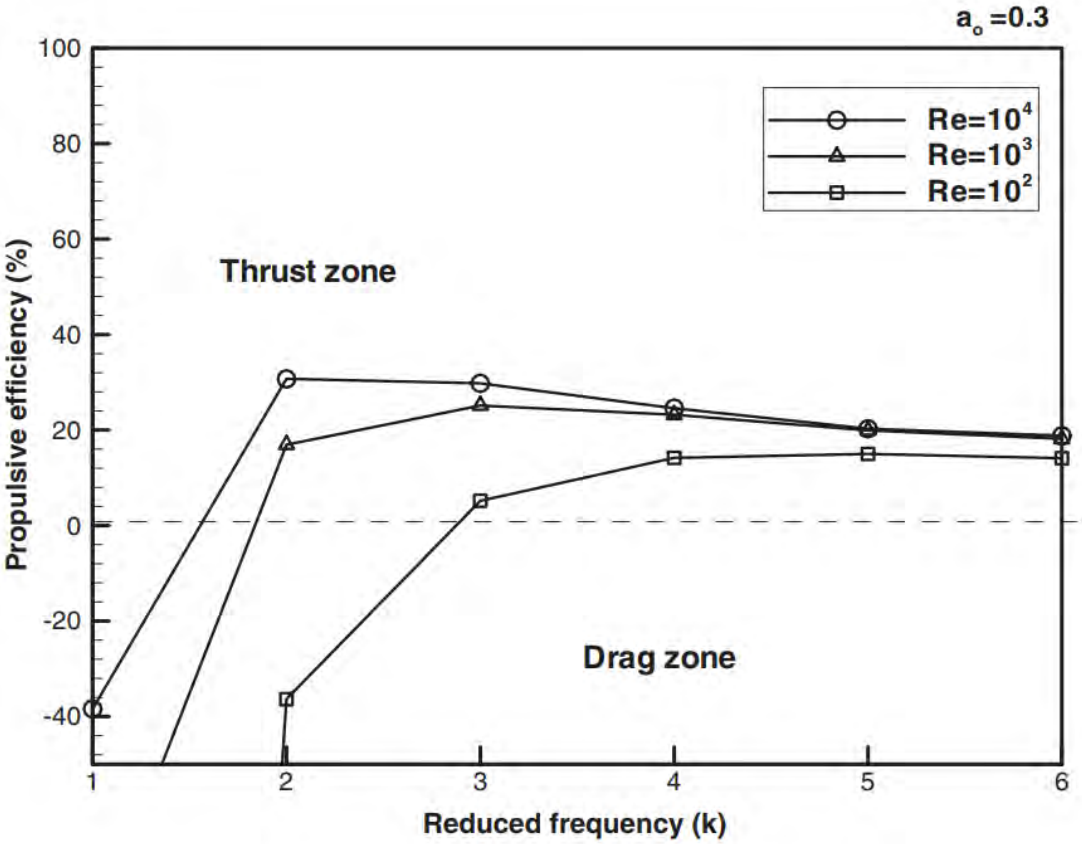

Figure 1. 10: The effect of reduced frequency on the propulsive efficiency. Figure is adapted from Miao (2006) [9]

Alexander J. Smits et al. (2017) provided scaling laws for thrust coefficient, power coefficient and propulsive efficiency for rigid foil undergoing pure heaving and pitching oscillations. Alexander J. Smits et al. (2017) also studied the dependence of propulsive performance of pure heaving and pure pitching airfoil on waveform. They used Jacobi elliptic functions (k) to define different waveforms and found that in the heaving oscillation, the thrust coefficient is almost same for all waveform, but there is a sudden rise in its value as the waveform approaches square waveform (Figure 1.9). The reason provided for this is the release of vortex pairs from the trailing edge instead of single vortices as in the case of other waveform (Figure 1.10). While in pitching oscillation thrust coefficient in square waveform is also almost similar to that in sinusoidal and triangular waveform as the secondary vortex in pitching is very weak in comparison to primary vortex.

.

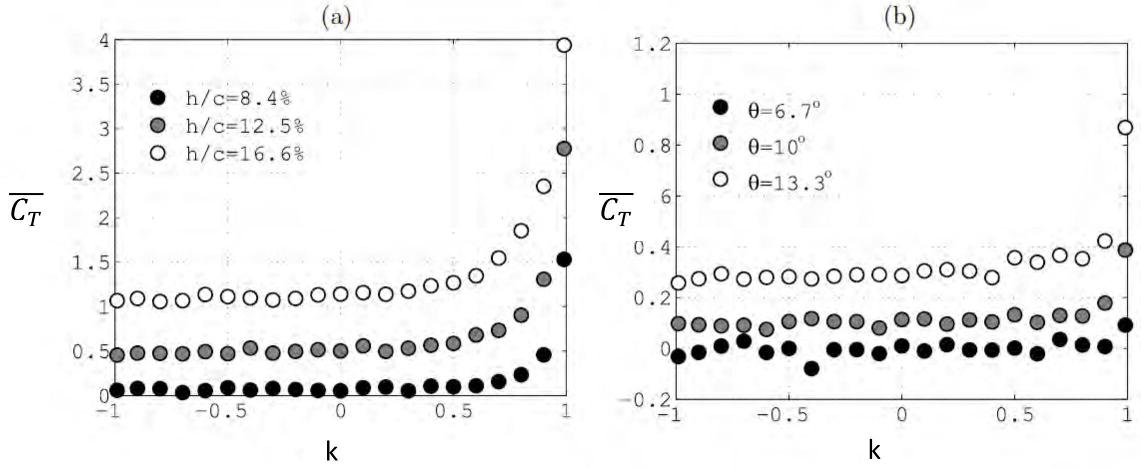

Figure 1. 11: Variation of thrust coefficient for (a) heaving and (b) pitching foil with elliptic modulus (k) [10]

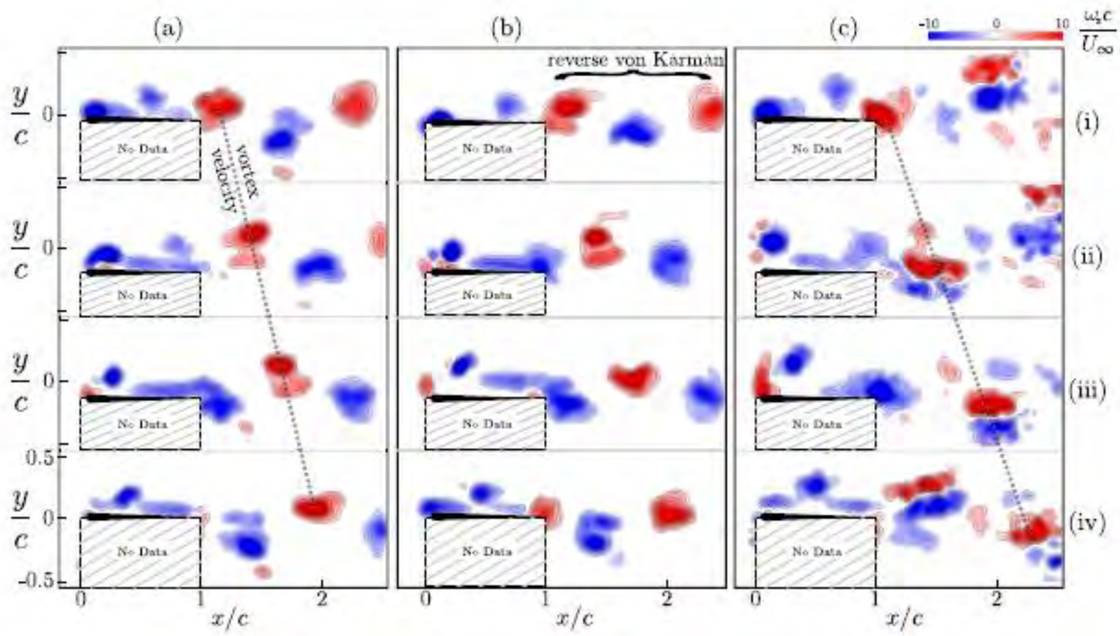

Figure 1. 12: Heaving motions, phase-averaged spanwise vorticity, h_0/c = 12.5%, St = 0.4. Waveform types: (a) triangular-like k = −0.99; (b) sinusoidal k = 0; (c) square-like k = 0.99. Phases: (i) φ = 0^0; (ii) 90^0; (iii) 180^0; (iv) 270^0 [10]

M. Jimreeves David et al. (2017) has studied thrust generation from pitching foils with flexible flap attached to its trailing edge. At k = 6, he found the peak mean thrust coefficient to be about 100 % higher than the rigid foil thrust and occurs at $R*$ value of approximately 8, while the peak efficiency is found to be approximately 300 % higher than the rigid foil efficiency and occurs at a distinctly different $R*$ value of close to 0.01 (Figure 1.11). Corresponding to these two optimal flexural rigidity parameter values, he found two distinct flap deflection shapes; the peak thrust corresponding to a mode 1 type simple bending of the flap with no inflection points, while the peak efficiency corresponds to a distinctly different deflection profile having an inflection point along the flap.

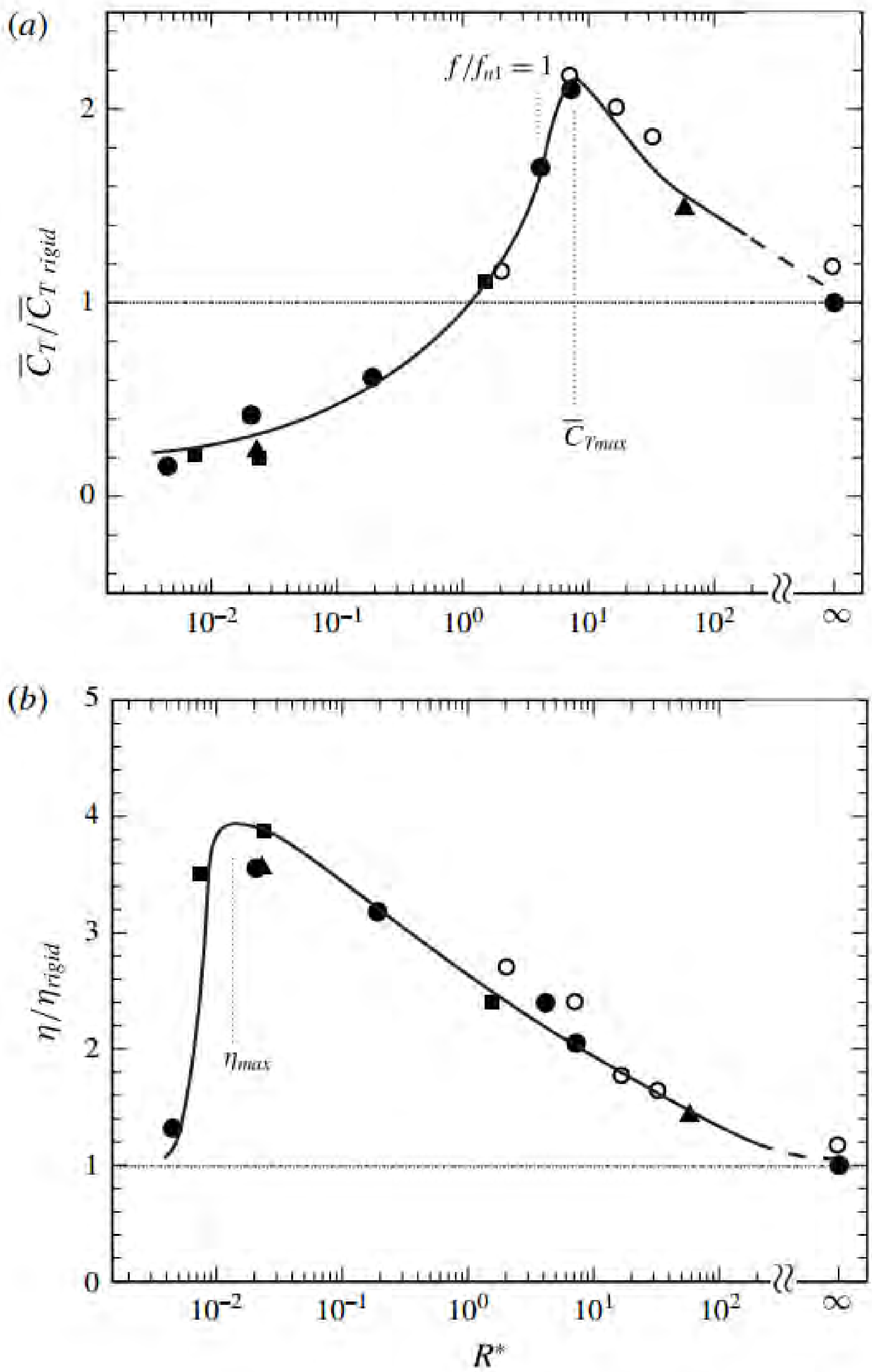

Figure 1 .11: Variation of (a) the time-averaged thrust and (b) the propulsive efficiency (η) versus non-dimensional rigidity parameter (R∗). Both thrust and efficiency values shown are normalized by the corresponding value for the rigid foil at the same k (k ≈ 6).

He also presented the cycle-averaged total thrust (C_T) and the individual contributions from both normal (C_{TN}) and axial (C_{TA}) forces as a function of the reduced frequency. As one might expect, for rigid foil the normal force contribution to thrust is much larger than the axial force contribution, the ratio between the two being a factor of approximately 8 at a k of around 10. The total thrust (C_T) is thus very close to the contribution from the normal force (C_{TN}), with the values being a little lower due to the negative contribution (or drag) from the axial force (Figure 1.12).

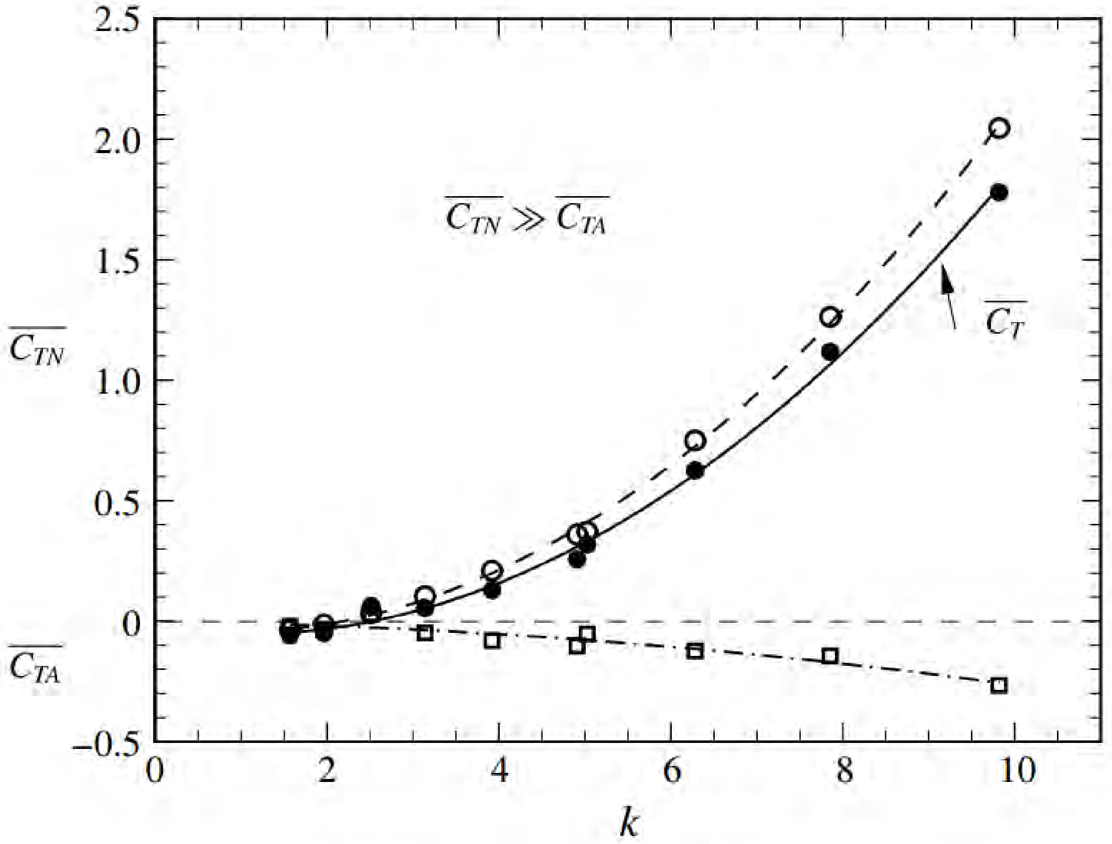

Figure 1 .12: Variation of the time-averaged thrust with reduced frequency for the rigid foil (θ_{max} = 10 ∘). The contributions to thrust from both the normal force (C_{TN}) and the axial force (C_{TA}) are shown, in addition to the total thrust (C_T). The main contribution to thrust is from the normal force (C_{TN}) with small negative values from the axial (C_{TA}).

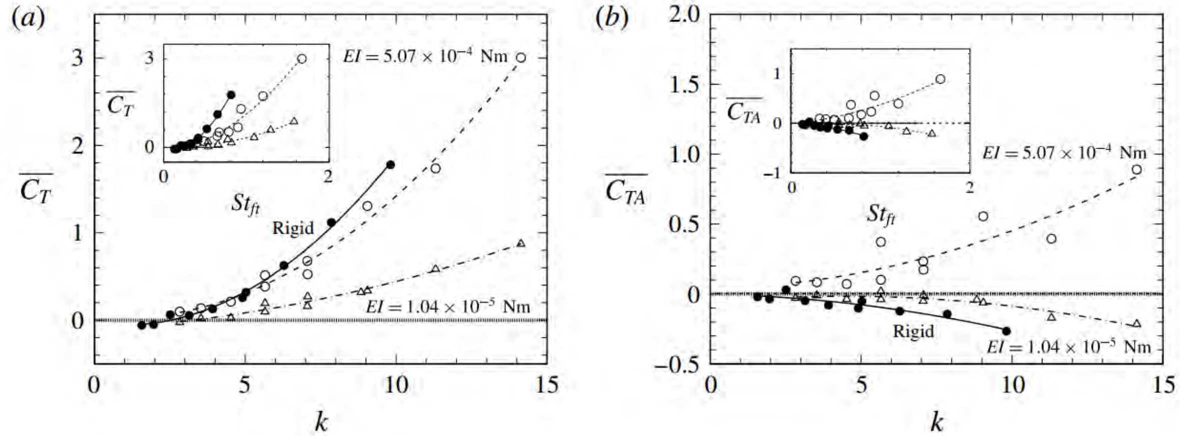

Figure 1.13: Time-averaged thrust coefficient variation with reduced frequency k for flexible foils. In (a), the total thrust coefficient (C_T) is shown, while in (b), the contribution to thrust from the axial force (C_{TA}) is shown. The data are plotted with the reduced frequency (k) in the main plot, and with the Strouhal number (St) formed using the excursion of the flexible flap trailing edge in the inset plots. The EI = 5.07 × 10−4 Nm case stands out as it shows reasonably large positive values of C_{TA}. In both flexible cases, the ratio of the flexible flap to total chord (c_F/c) is 0.45.

He also shown that in contrast to the above result, contribution of axial thrust to the total thrust is considerable for flexible foil (Figure 1 .13). The rigid foil case and the lower flexural rigidity case, both show negative values of C_{TA}, while the foil with EI = 5.07 × 10−4 Nm has relatively large positive values of C_{TA}. Infact the axial force contribution to thrust (C_{TA}) at reduced frequency of approximately 14 is close to 1 for the EI = 5.07 × 10−4 Nm foil case, which is approximately one third of the total thrust generated in this case.

Alexander J. Smits et al. (2017) also presented that pitching and heaving foils can not be adequately described using only the Strouhal number or the reduced frequency. Figure 1 .14 shows the time-averaged thrust coefficient as a function of Strouhal number for a heaving foil. We see that the ratio of the heave amplitude to chord, h∗ = h_0/c, has a significant impact on the thrust generated at a fixed Strouhal number.

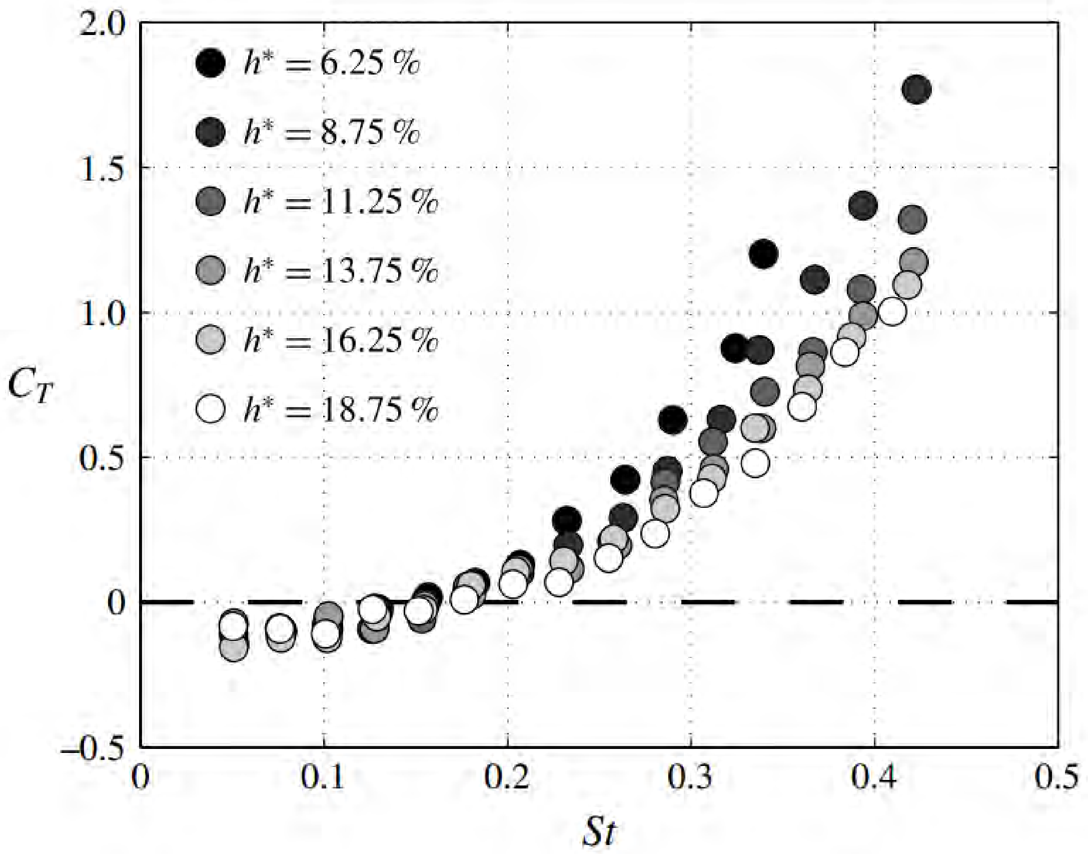

Figure 1 .14 Time-averaged thrust coefficient C_T as a function of Strouhal number St for a heaving foil, for various heave amplitude to chord ratios, h∗.

1.4 Present work

In the present work, we have performed experiments on pure heaving foil in sinusoidal waveform. Study has been done on both rigid NACA 0012 foil and foil attached with flexible flap at its trailing edge. Work consists of two stages. In the first stage we have performed experiments at lower heave amplitude ($h_0/c = 0.11$) and in the later part of the work, higher heave amplitude to chord ratio ($h_0/c = 0.32$) has been studied.

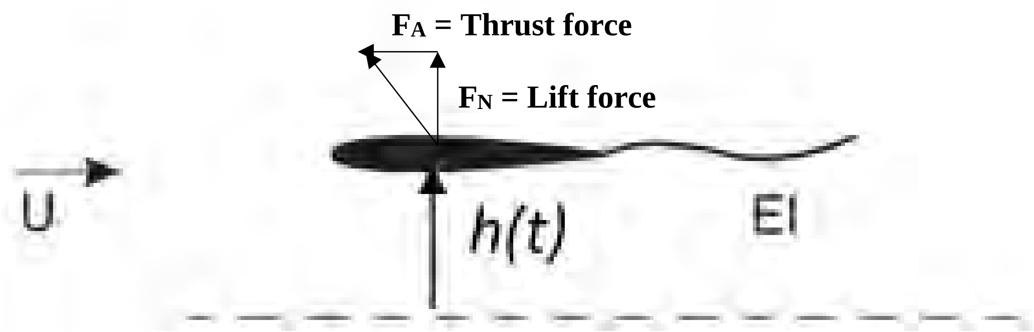

Figure 1. 15: Schematic showing thrust and lift force

Result obtained is then compared with the result on pure pitching foil of M. Jimreeves David with maximum pitching amplitude of 10^0.

Calculation of parameters

We measure forces normal to the foil F_N and force along the foil F_A (chord wise). We normalized the force with $0.5\rho u^2 sc$ where s is the span and c is the total chord of the foil. In case of flexible foil total chord is the sum of rigid chord (c_R) and flexible chord (c_f). Normalized version of F_N is C_{FN} and for F_A is C_{FA}.

$$C_{FA} = \frac{F_A}{0.5\rho u^2 sc}, \quad C_{FN} = \frac{F_N}{0.5\rho u^2 sc}$$

Power is calculated as the product of instantaneous normal force, F_N and corresponding heave velocity. Power, P is normalized as

$$C_P = \frac{P}{0.5\rho u^3 sc}$$

Propulsive efficiency of the foil is given by,

$$\eta = \frac{\overline{C_T}}{\overline{C_P}}$$

2 Experimental Methods

Airfoil immersed in flowing water inside a water tunnel are oscillated with scotch-yoke mechanism driven by a three-phase induction motor. A load cell is mounted over the air-foil to measure force. The linear positions of the blade is measured through calibrated rotary potentiometers.

2.1 Water tunnel

The water tunnel consists of a test section of cross-section 0.45m (height) × 0.26m (width) and is 1.2*m* long. The maximum speed of the tunnel is 30 cm/sec. The tunnel is closed circuit type with a contraction ratio of 6. The speed of the water flow can be adjusted by a controller, which controls the speed (rpm) of the pump. The water tunnel has been calibrated using *PIV* by Chatterjee. A (2009) and the calibration value was found to be 0.01 *cm/sec/rpm*. The mean flow in the test-section is hence determined from the rpm setting of the pump.

2.2 Experimental Setup

The experimental setup consists of an Airfoil (NACA0012) of chord 12.5cm and aspect ratio 2.4 immersed in flowing water and driven by a digital servo motor to achieving pitching motion about its quarter chord, with a load cell to measure the unsteady forces and moments on the foil and a potentiometer to measure angular positions.

2.2.1 Scotch-Yoke mechanism

A scotch-yoke mechanism (figure 3.1) is used to convert the rotary motion from motor to linear motion of the airfoils. Scotch-yoke mechanism generates sinusoidal motion. The rota-trigonal motion of the wheel is converted to linear motion of the yoke.

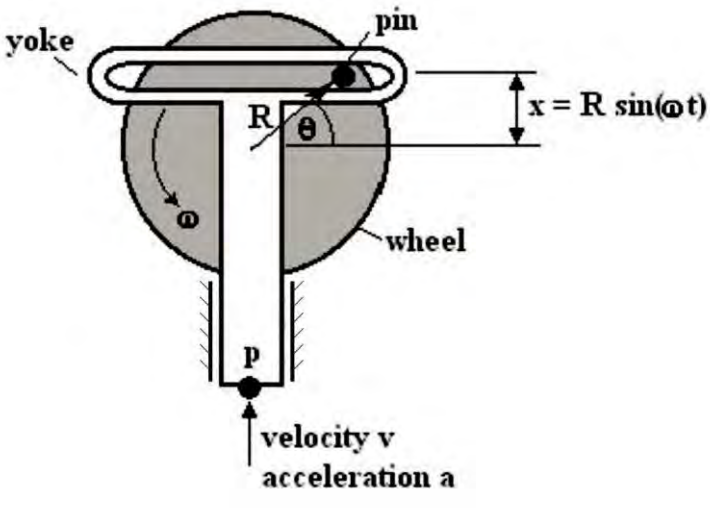

Figure 2. 1 : Schematic of scotch-yoke setup

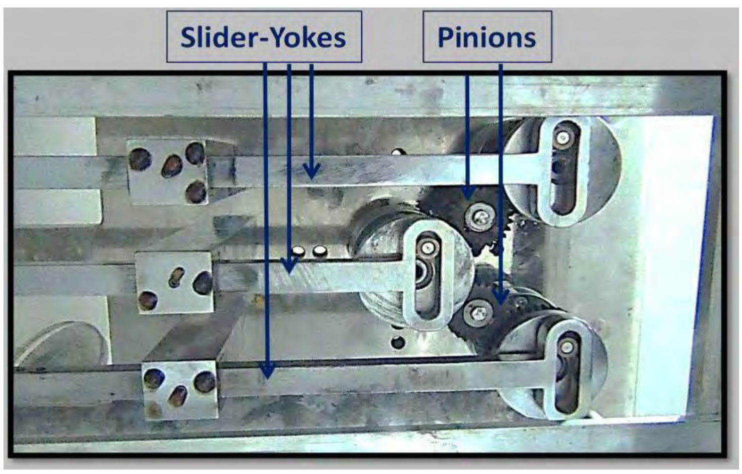

Figure 2. 2: Scotch-yoke used in Mechanism

2.2.2 Motor and Controller

The motor used is 0.5 HP and it has a B5 type mounting (flange mounting). Rated speed of the motor is 1400 rpm. The running speed of the motor is controlled by a controller. The ECO101M type 1.6 KVA controller receives single phase AC input and provides 3 phase output to the motor. The operating speeds of the motor at which the experiments are performed, are very low. The motor does not provide enough torque to drive the whole mechanism at very low speeds. In order to overcome this problem, a helical-worm gearbox with fixed speed reduction of 60:1 is used. The helical gears ensure smooth operation, while providing sufficient torque. A flexible sleeve type coupling is used to connect the gear box output to the shaft of gear which is connected to central airfoil. The motor and the controller are shielded with a copper foil and the foil is connected to the ground so as to reduce the electro-magnetically induced noise in the load cell. Figure 3.3 and 3.4 show the motor, controller and the reduction gears used.

Figure 2. 3: Motor and controller

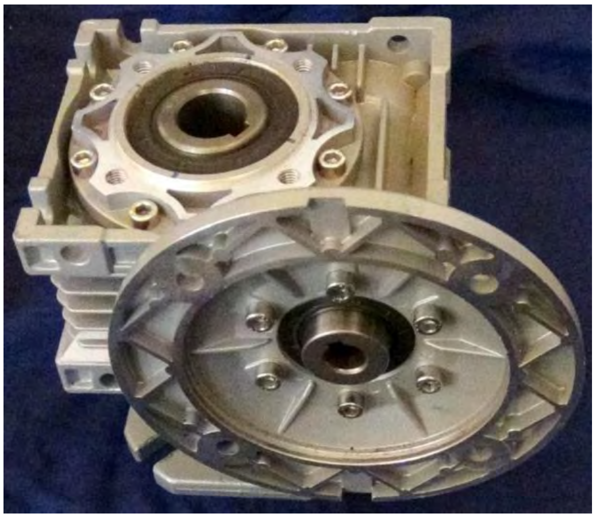

Figure 2. 4: 60:1 reduction gearbox

2.2.3 Force and Moment Measurement

In the oscillating foil experiments, it is necessary to measure the chord-wise and normal force to get the lift and drag curves for the foil. In oscillating foil experiments, the moment is measured to calculate the power transferred between the blade and the fluid. Load cell is used to measure force as well as moment exerted on the blade. The measurements of comparatively tiny drag or forces are susceptible to drift and random fluctuations. To achieve precise reading, we take cycle average of about 100 oscillation cycles. We take zero readings before and after each run and to account for any drift in between the experiment we take interpolated zero readings which are subtracted from pitching force reading. To prevent spurious electrical signals from motor corrupting load cell force signals, we completely isolate the load cell electrically by sandwiching it in between two acrylic blocks, so there is no electric contact with the rest of the system.

2.2.4 Load Cell

We are using a 6-axis ATI-mini 40 load cell to get forces (Fx, Fy, Fz) and moments (Mx, My, Mz). A DC power supply of 5-volt, input current 260 mA is given to the load cell. The load cell has two sides, the tool side (foil fits here) and mounting side (motor side).

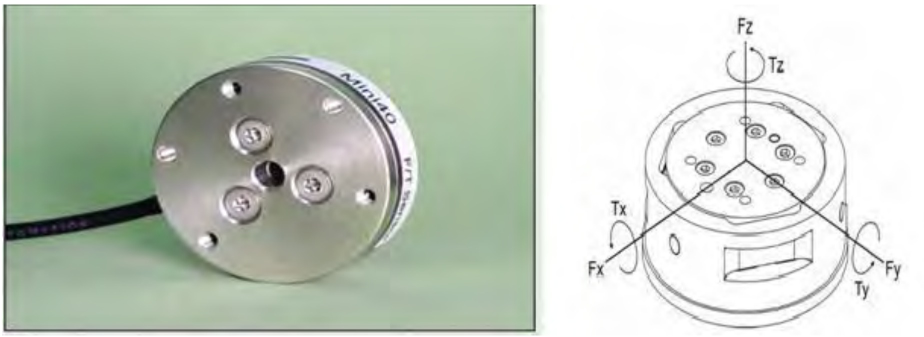

Figure 2. 5: ATI min 40 load cell

Calibration Range of Load cell

	Fx (N)	Fy (N)	Fz (N)	Tx (Nm)	Ty (Nm)	Tz (Nm)
Range (+/-)	20	20	60	1	1	1
Resolution (+/-)	0.005	0.005	0.01	0.000125	0.000125	0.000125

Measurement uncertainty

Fx	Fy	Fz	Tx	Ty	Tz
1.25%	1.00%	0.75%	1.25%	1.25%	2.00%

2.2.5 Inertial correction

Forces and torque measured by the load cell is the combination of forces applied by water and inertial correction. Inertial correction is basically the force required to move the weight underneath the load cell. So, to get the actual thrust generation and power, inertial correction must be subtracted from the recorded values. Inertial correction is calculated by running the set-up in air and calculating the forces, assuming forces applied by air on the foil is significantly lower in comparison to inertial correction values. Inertial correction or mass underneath the load cell is given by the slope of the curve plotted between amplitude of F_y and $h_0\omega^2$. The calculated value of inertial correction is 0.62 which is found to be same as the measured mass of the foil and other components below the load cell.

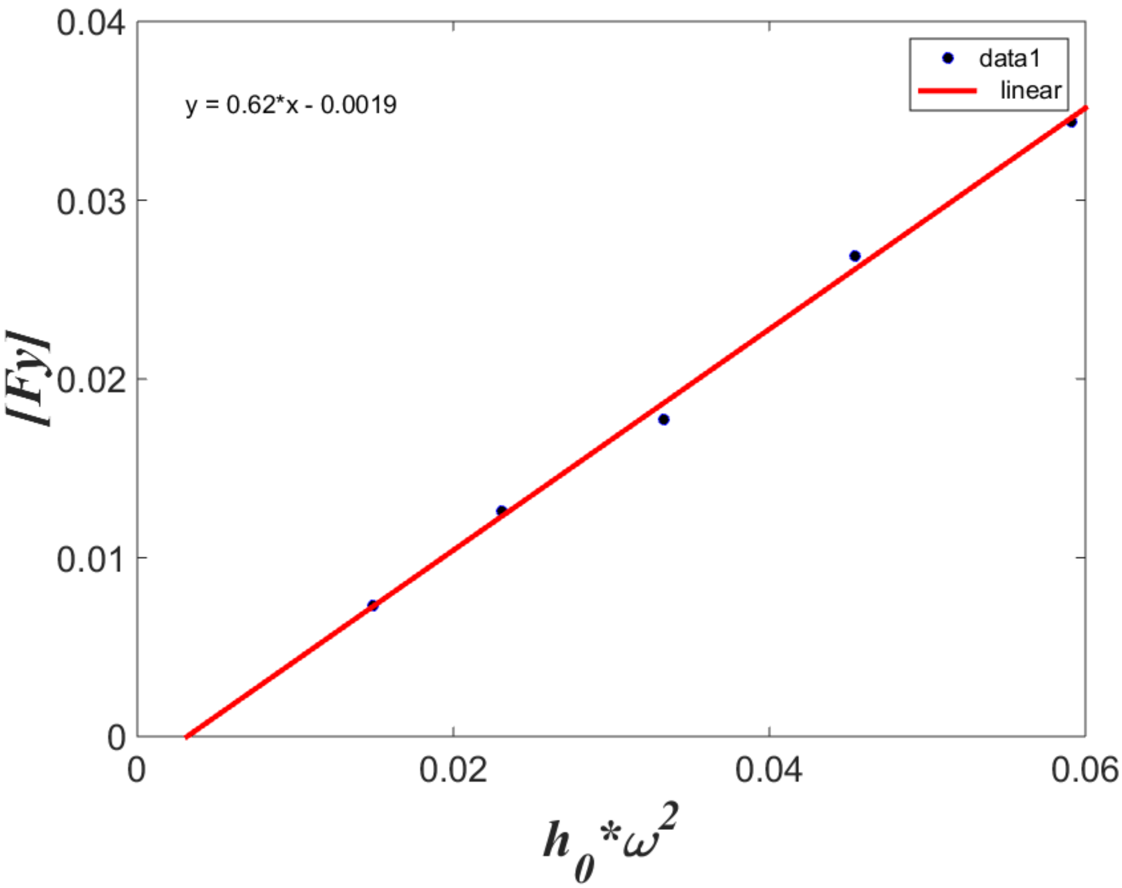

Figure 2. 6: Calculation of inertial correction of the set-up.

2.2.6 Linear displacement measurement

In the present work, capacitor based linear displacement sensor has been used. Capacitive sensors (capacitive linear displacement sensors) are noncontact devices capable of high-resolution position measurement and/or position change - displacement measurement - of any conductive target. Capacitive sensors use the electrical property of "capacitance" to make measurements. Capacitance is a property that exists between any two conductive surfaces within some reasonable proximity. Changes in the distance between the surfaces changes the capacitance. It is this change of capacitance that capacitive sensors use to indicate changes in position of a target. The displacement sensor can sense the position up to 8 mm, but for proper functioning, it is placed well below 5mm from the target.

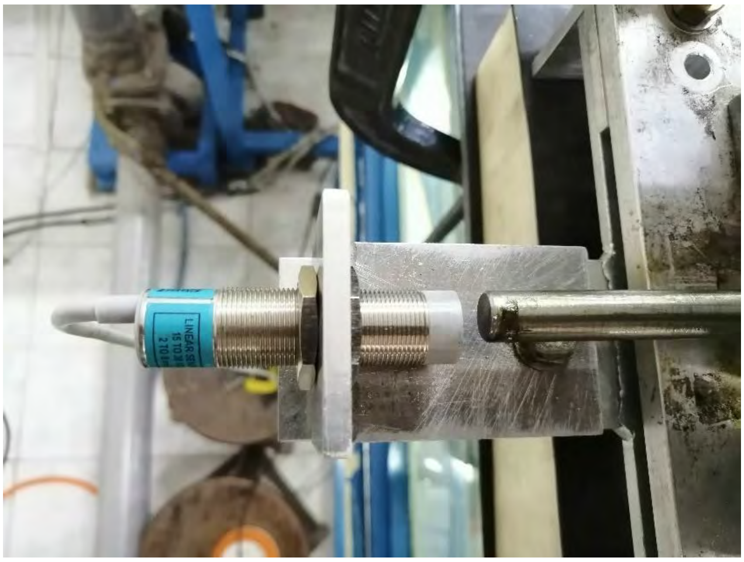

Figure 2. 7 : Capacitive linear displacement sensors used in experiments

3 Experimental Results

In this chapter, we present the propulsive parameters (thrust, power, efficiency) measured in heaving of rigid foil at two different amplitude of oscillations with and without flexible flap attached at its trailing edge.

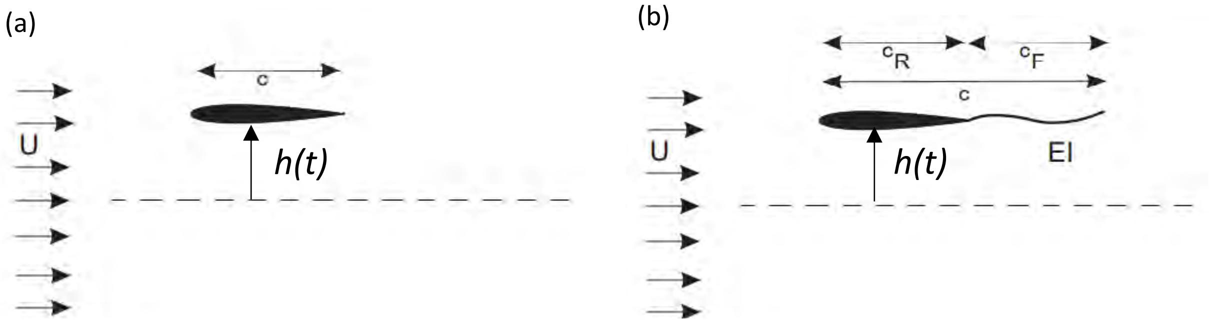

Figure 3.1. Schematic showing heave oscillation of (a) rigid foil (b) rigid foil attached with flexible flap at its trailing edge.

3.1 Non-dimensional numbers

The main length scales in the present problem are the foil chord, c, and the peak to peak excursion of the foil tip, A, which is twice the heave amplitude while the main velocity scales are the free-stream velocity, u and oscillation frequency, f.

Non-dimensional numbers	
Reynolds number (Re)	Re = uc/ν
Strouhal number (St)	St = fA/u
Flexural rigidity Parameter (R^*)	$R^*=\frac{EI}{0.5\rho u^2 {C_f}^3}$

Table 3.1. Non-dimensional numbers in the study

In the present study experiments are performed at constant free-stream velocity of 5 cm/s and frequency is varied using required combination of induction motor speed and gearbox to achieve the desired values of Strouhal number, keeping in account load cell limits. Input parameters are kept in the following range.

Re ~ 7000 to 14000 f ~ 0.05 to 1.2 Hz

3.2 Rigid foil

In the present study, measurements of the parameters have been done for a rigid NACA0012 foil having chord length, c=12.5cm and undergoing heave oscillation with amplitude of 13.5 and 40 mm respectively. Maximum efficiency of 27% has been attained for $h_0/c = 0.32$ (corresponding to 40 mm heave amplitude) at St = 0.28 (Figure 3.2). The value of thrust coefficient, C_T at the corresponding St is 0.35 (Figure 3.3). The results obtained are also compared with pure pitching oscillation with $\theta_0 = 10^0$ done by M. Jimreeves (2017).

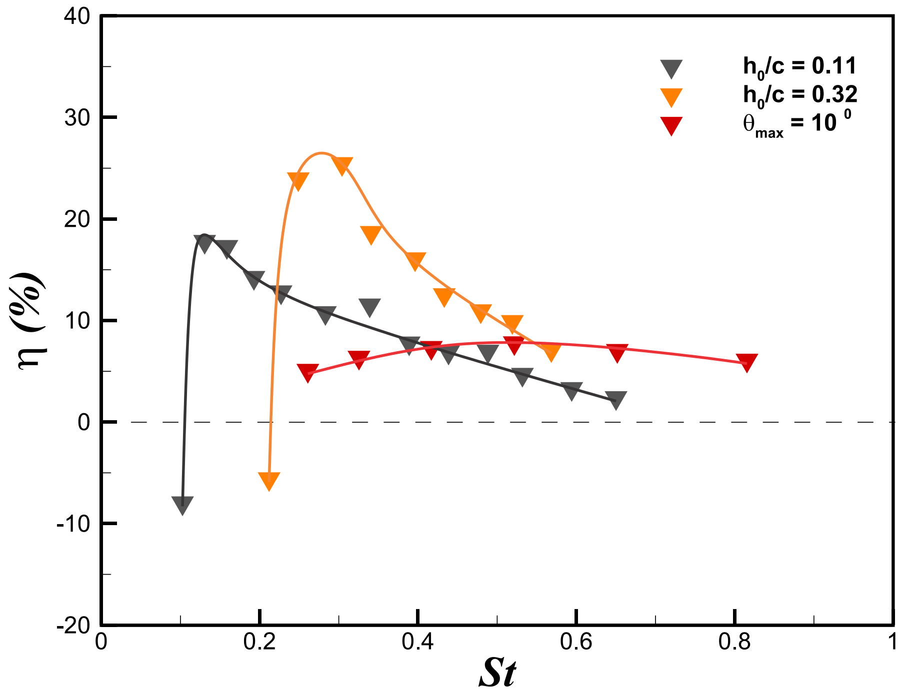

Figure 3.2. Rigid foil. Efficiency, η as a function Strouhal number, St for heaving foil with $h_0/c = 0.11$, $h_0/c = 0.32$ and Jimreeves result on pure pitching with $\theta_{max} = 10^0$.

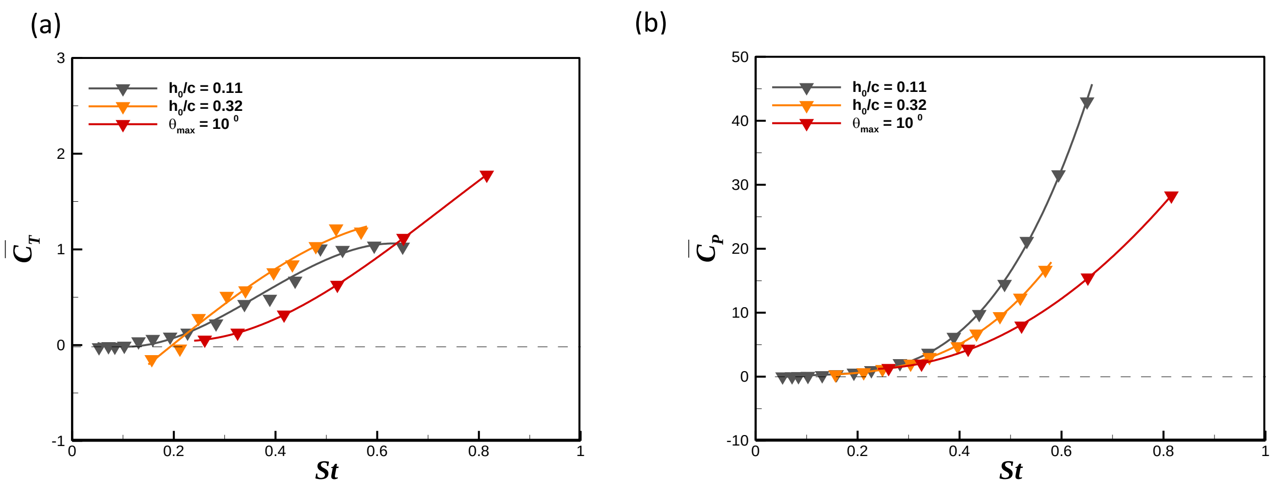

Figure 3.3. Rigid foil. (a) Mean thrust coefficient, $\overline{C_T}$ and (b) power coefficient, $\overline{C_P}$ as a function of St for h_0/c =0.11 and 0.32 and Jimreeves result on pure pitching with $\theta_{max} = 10^0$.

3.3 Flexible foils

The flexible foil is constructed by attaching a flexible flap of length C_F to the trailing edge of rigid foil (chord length C_R). This configuration of the flexible foil brings in two additional parameters, namely flexural rigidity of flexible flap (*EI*) and the ratio of the flexible flap length to the total chord length ($\frac{C_F}{C}$). The flexural rigidity EI may be normalized to yield a non-dimensional flexibility parameter R^*, defined as

$$R^*=\frac{EI}{0.5\rho u^2 {C_F}^3}$$

In this flexibility study all the forces and power are normalized using total chord (C=$C_F + C_R$).

The flexural rigidity (*EI*) of the flap is measured by overhanging various amount of the flap and measuring the corresponding flap tip deflection (δ), due to its self-weight. It is calculated from the formula for a cantilever beam with a uniformly distributed load (UDL):

$$EI = \frac{wl^4}{8\delta}$$

Where, *w* is self-weight of the flap per unit length, *l* is amount of overhang, *E* is the Young's modulus of the flap material and *I* is the area moment of inertia of the flap cross-section.
Where, w is self-weight of the flap per unit length, l is amount of overhang, E is the Young's modulus of the flap material and I is the area moment of inertia of the flap cross-section. We have done experiments for a range of R* varying from 0.0044 to 4.73 and $\frac{C_F}{C} = 0.45$ to study the effect of flexibility with two different heave amplitude to chord ratio (h_0/c).

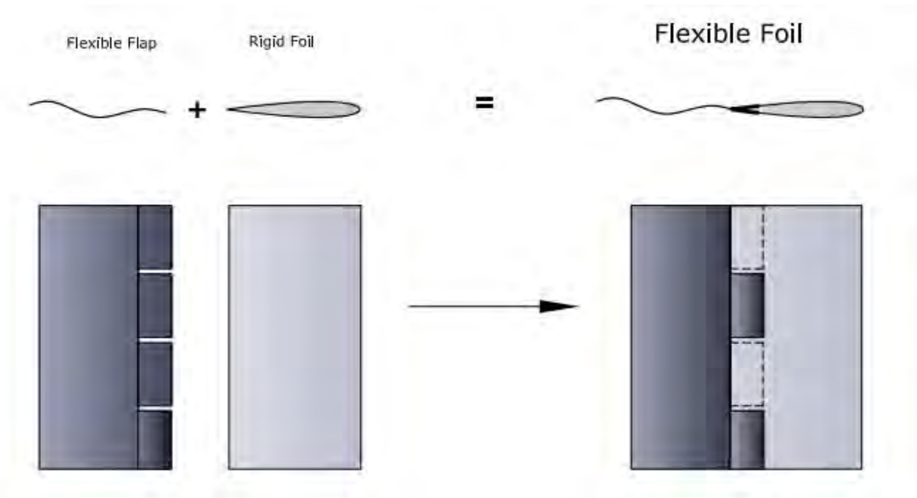

Figure 3.4. Schematic showing construction of flexible foil.

3.3.1 R* = 0.0044

In this case, maximum efficiency attained for $h_0/c = 0.11$ is 28% which is higher in comparison to $h_0/c = 0.32$ (24%). But corresponding C_T for $h_0/c = 0.32$ is 0.2 while that for $h_0/c = 0.11$ is 0.08, which is very less. Even from figure 3.5, it seems that C_T is increasing with Strouhal number up to St ~ 0.5 for both the cases, attaining a maximum value and after that it starts decreasing.

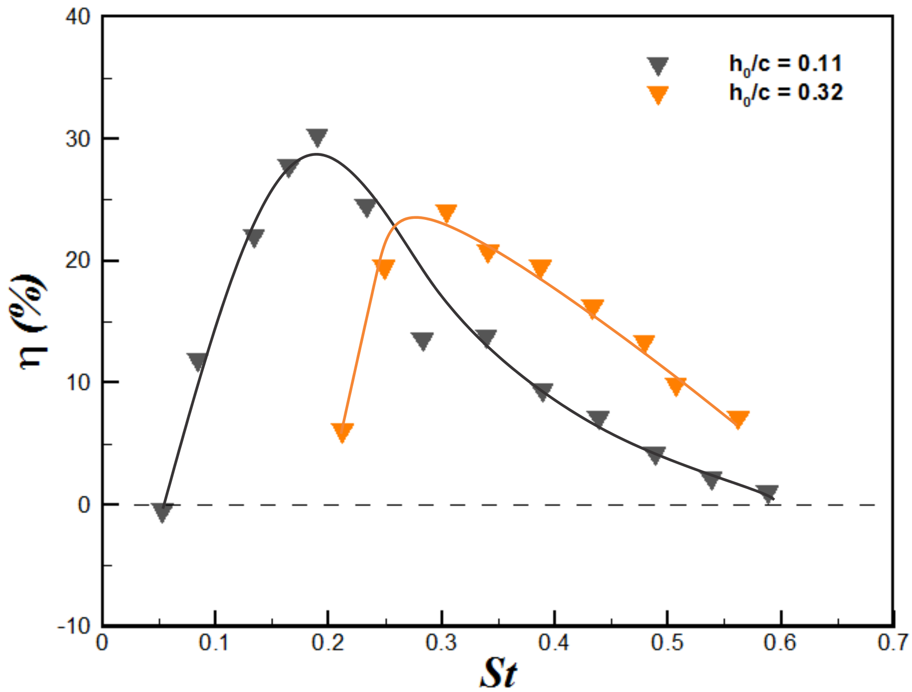

Figure 3.5. R* = 0.0044. Efficiency, η as a function Strouhal number, St for heaving foil with $h_0/c = 0.11$, $h_0/c = 0.32$.

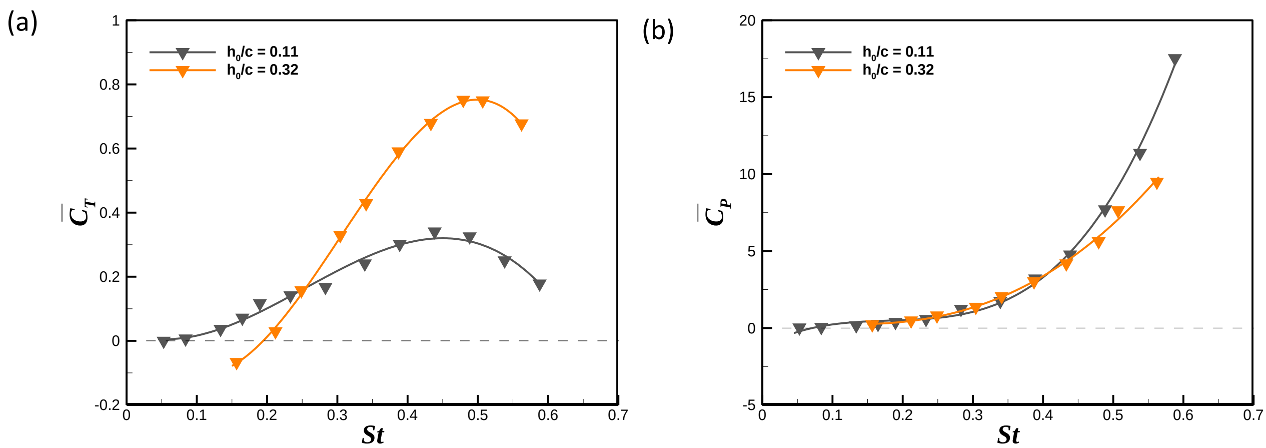

Figure 3.6. R* = 0.0044. Variation of (a) thrust coefficient, C_T and (b) power coefficient, C_P with Strouhal number, St for $h_0/c = 0.11$, $h_0/c = 0.32$.

3.3.2 R* = 0.473

In this case also the maximum efficiency is higher for $h_0/c = 0.11$ in comparison to $h_0/c = 0.32$ and same as the previous case the corresponding C_T for $h_0/c = 0.11$ is significantly small. For $h_0/c = 0.11$, the slope of C_T is very small before St = 0.22 and then increases sharply afterwards, while in contrast there is no sudden increase in C_T for $h_0/c = 0.32$. In the figure 3.6 and 3.7 the results are also compared with M. Jimreeves work on pure pitching.

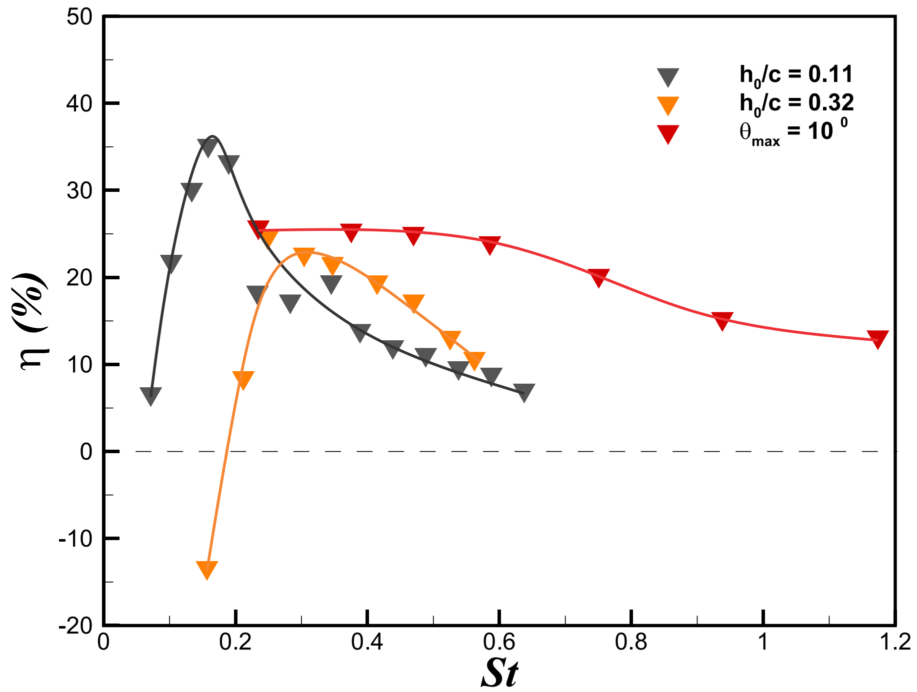

Figure 3.7. R* = 0.473. Efficiency, η as a function Strouhal number, St for heaving foil with $h_0/c = 0.11$, $h_0/c = 0.32$ and Jimreeves result on pure pitching with $\theta_{max} = 10^0$.

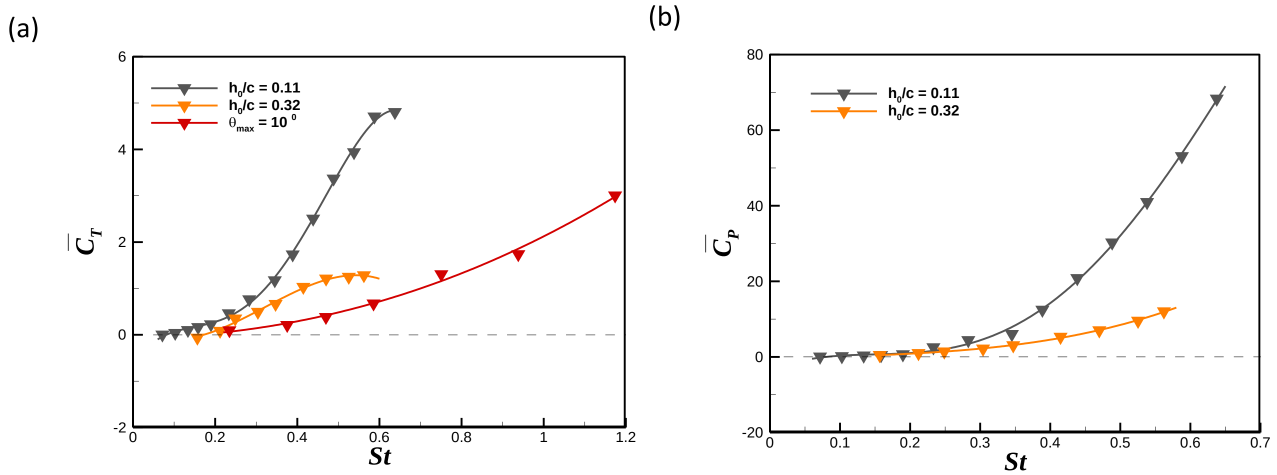

Figure 3.8. R* = 0.473. (a) Mean thrust coefficient, $\overline{C_T}$ and (b) power coefficient, $\overline{C_P}$ as a function of St for h_0/c =0.11 and 0.32 and Jimreeves result on pure pitching with $\theta_{max} = 10^0$.

3.3.3 Variation of parameters with R*

To have a better understanding of the effect of flexibility on thrust coefficient and efficiency, normalized thrust coefficient at a fixed Strouhal number has been studied as a function of R*. Normalization being done with the rigid foil thrust coefficient at the same St. For $h_0/c = 0.11$, we have studied the variation of $\frac{C_T}{C_{T\,rigid}}$ as a function of R* at Strouhal number St = 0.16 (Figure 3.8).

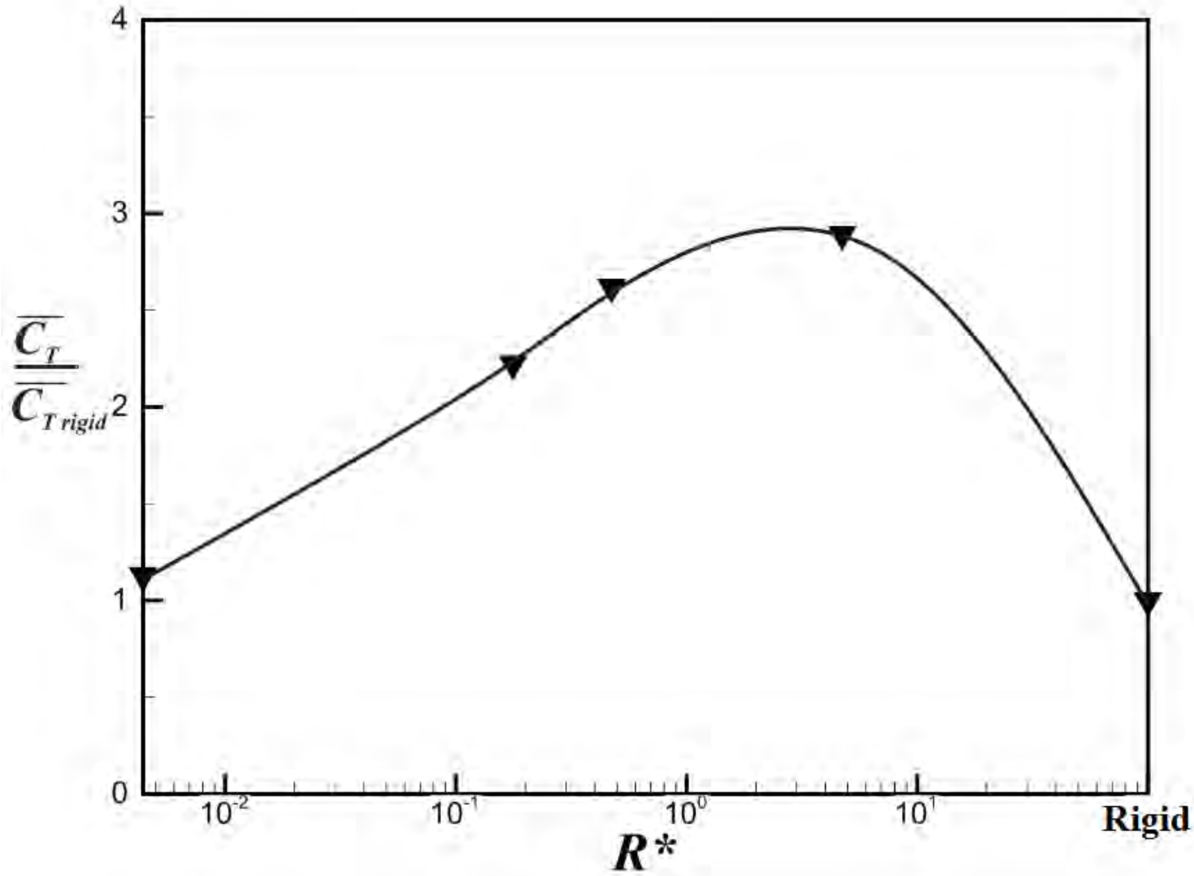

Figure 3.9: Variation of normalized thrust coefficient with R* at Strouhal number St = 0.16 for h_0/c = 0.11. Normalization being done with the rigid foil thrust coefficient at the same St.

As the R* of the foil increases, $\frac{C_T}{C_{T\,rigid}}$ initially increases and then it starts decreasing. The distinct flap deflection shape at different flexibility may be the reason for the pattern. It is to be noted that at the peak position, thrust coefficient is almost thrice the thrust coefficient of rigid foil.

Variation of $\frac{C_T}{C_{T\,rigid}}$ as a function of R* for $h_0/c = 0.32$ has also been studied at fixed Strouhal number St = 0.3. We found similar pattern in this case also, but maximum value of the thrust coefficient ratio is just above 1, which indicates that flexibility is not adding any advantage for higher heave amplitude. (Figure 3.9).

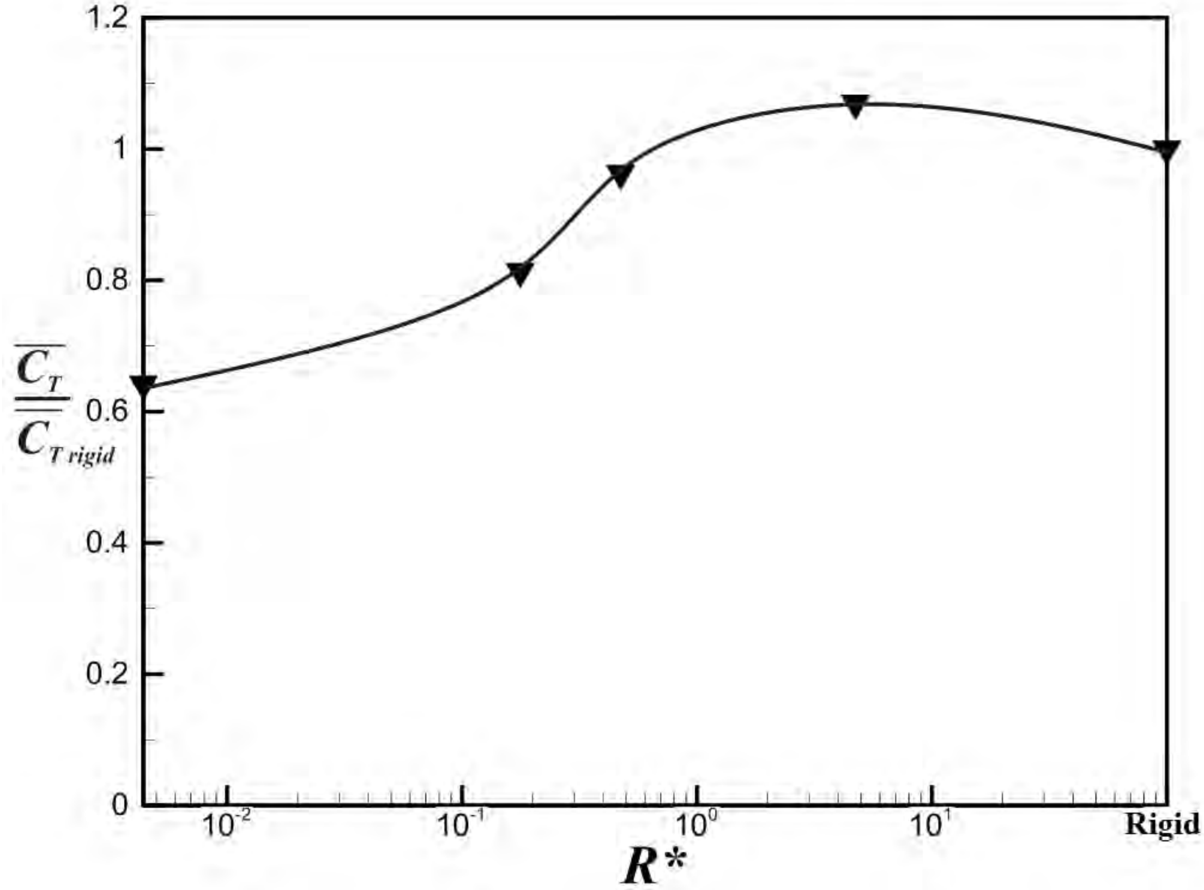

Figure 3.10: Variation of normalized thrust coefficient with R* at Strouhal number St = 0.3 for h_0/c = 0.32. Normalization being done with the rigid foil thrust coefficient at the same St.

For $h_0/c = 0.11$, normalized efficiency at Strouhal number, St = 0.16 also follows similar pattern when plotted against R*. Normalization being done with the rigid foil efficiency at the same St. The maximum value of $\frac{\eta}{\eta_{rigid}}$ is above 2, which means flexible foil is twice as efficient as rigid foil. But $\frac{\eta}{\eta_{rigid}}$ at St = 0.3 for the higher heave amplitude, $h_0/c = 0.32$ is dropping down with a rise in R*, reaching a minimum value of 0.6 and then again increases (Figure 3.11). The effect of leading edge vortices might be significant in the case and may be the probable reason for the pattern.

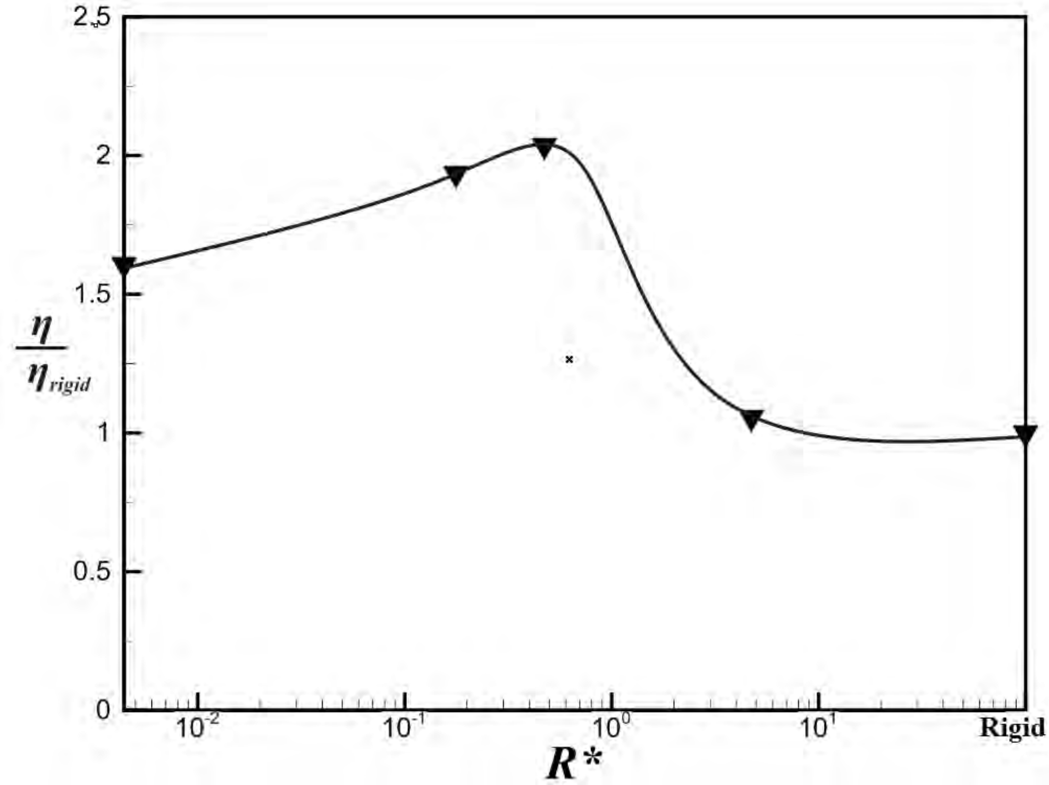

Figure 3.11: Variation of normalized efficiency with R* at Strouhal number St = 0.16 for $h_0/c = 0.11$. Normalization being done with the rigid foil efficiency at the same St.

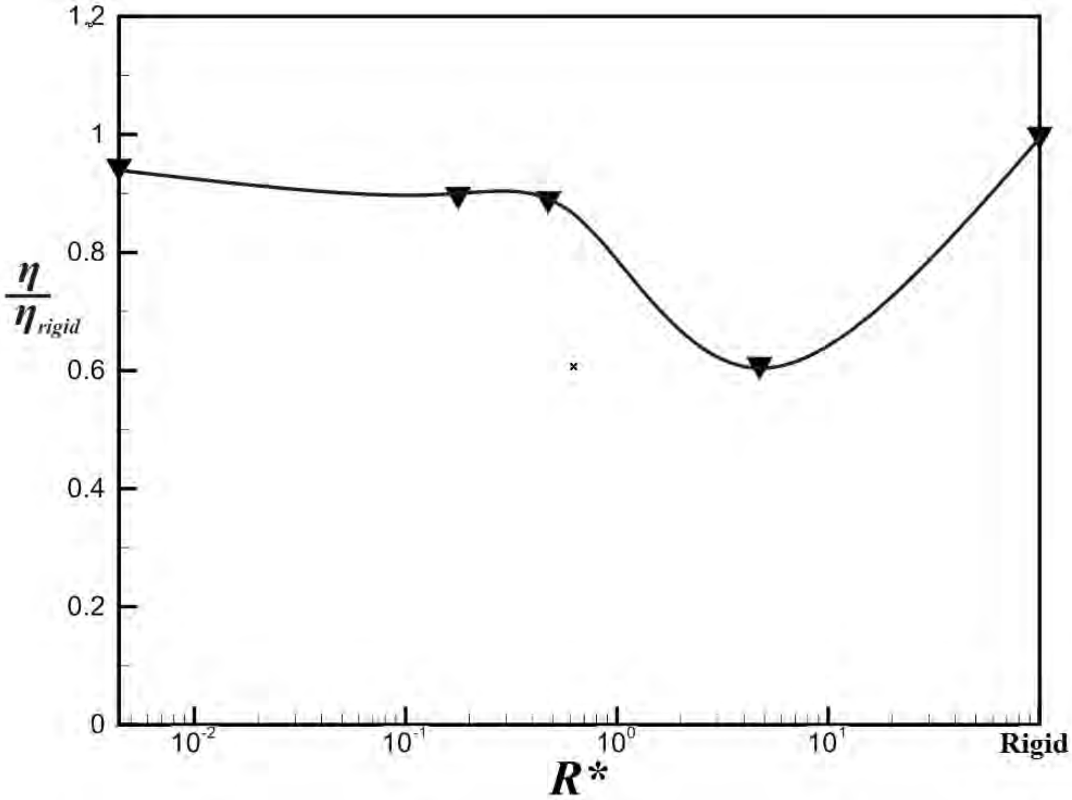

Figure 3.12: Variation of normalized efficiency with R* at Strouhal number St = 0.3 for $h_0/c = 0.32$. Normalization being done with the rigid foil efficiency at the same St.

3.4 Contour plot

To understand the combined effect of Strouhal number, St and flexibility on the parameters, we have made contour plots.

3.4.1 Efficiency

(a)

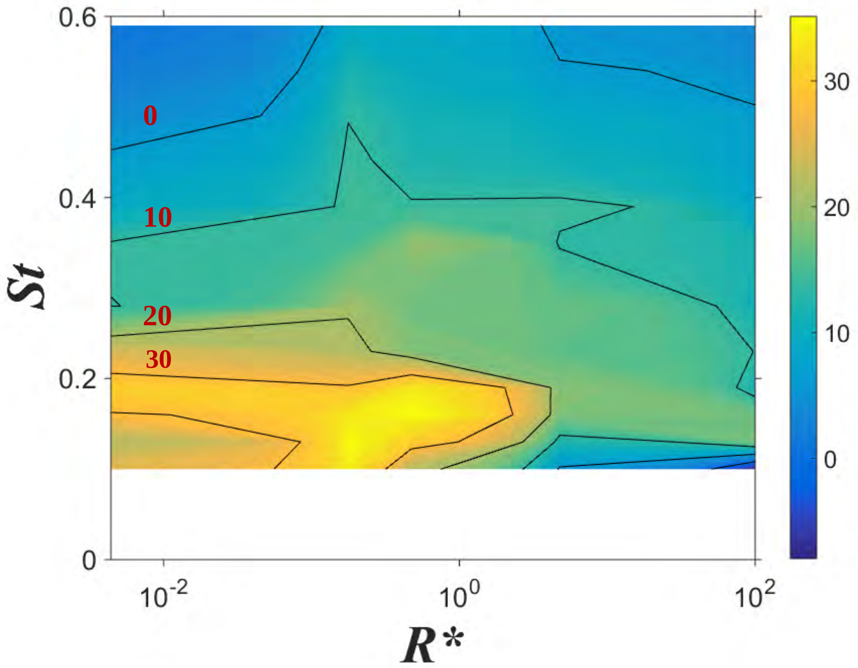

(b)

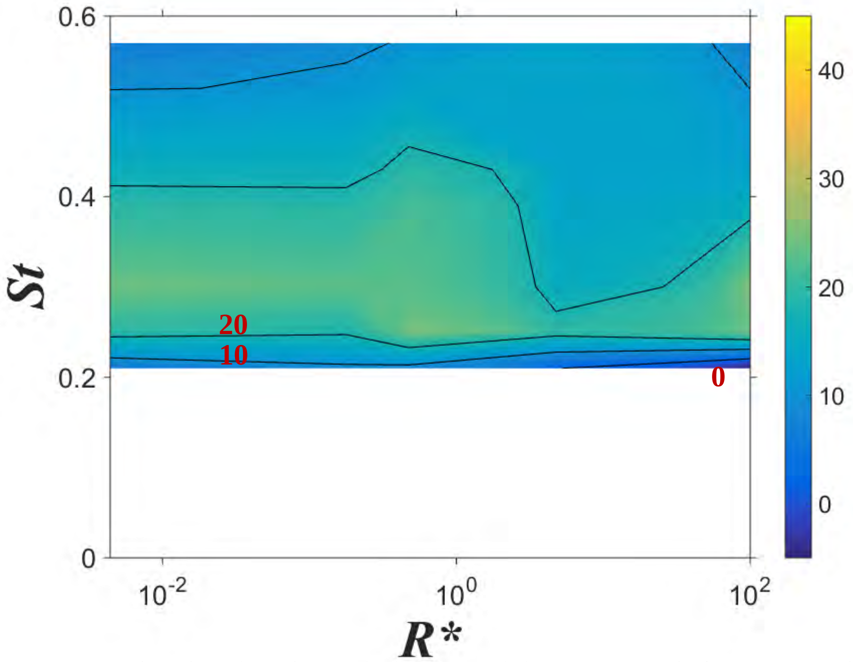

Figure 3.13. Contour plot showing the variation of efficiency for (a) $h_0/c = 0.11$ and (b) $h_0/c = 0.32$

For $h_0/c = 0.11$, efficiency is initially increasing with R*, reaching its maximum value at 0.473 and the again decreasing. However, the effect of R* is not seen in the case of higher heave, where maximum efficiency is always in the range of 20-25 % irrespective of R*.

3.4.2 Thrust coefficient

For $h_0/c = 0.11$, as efficiency thrust is also increasing with R*, reaching its maxima at R* = 0.473 and again starts decreasing. But in case of $h_0/c = 0.32$, maximum thrust coefficient is at R* = 4.73. As expected thrust coefficient is always increasing with Strouhal number for both h_0/c =0.11 and 0.32.

(a)

(b)

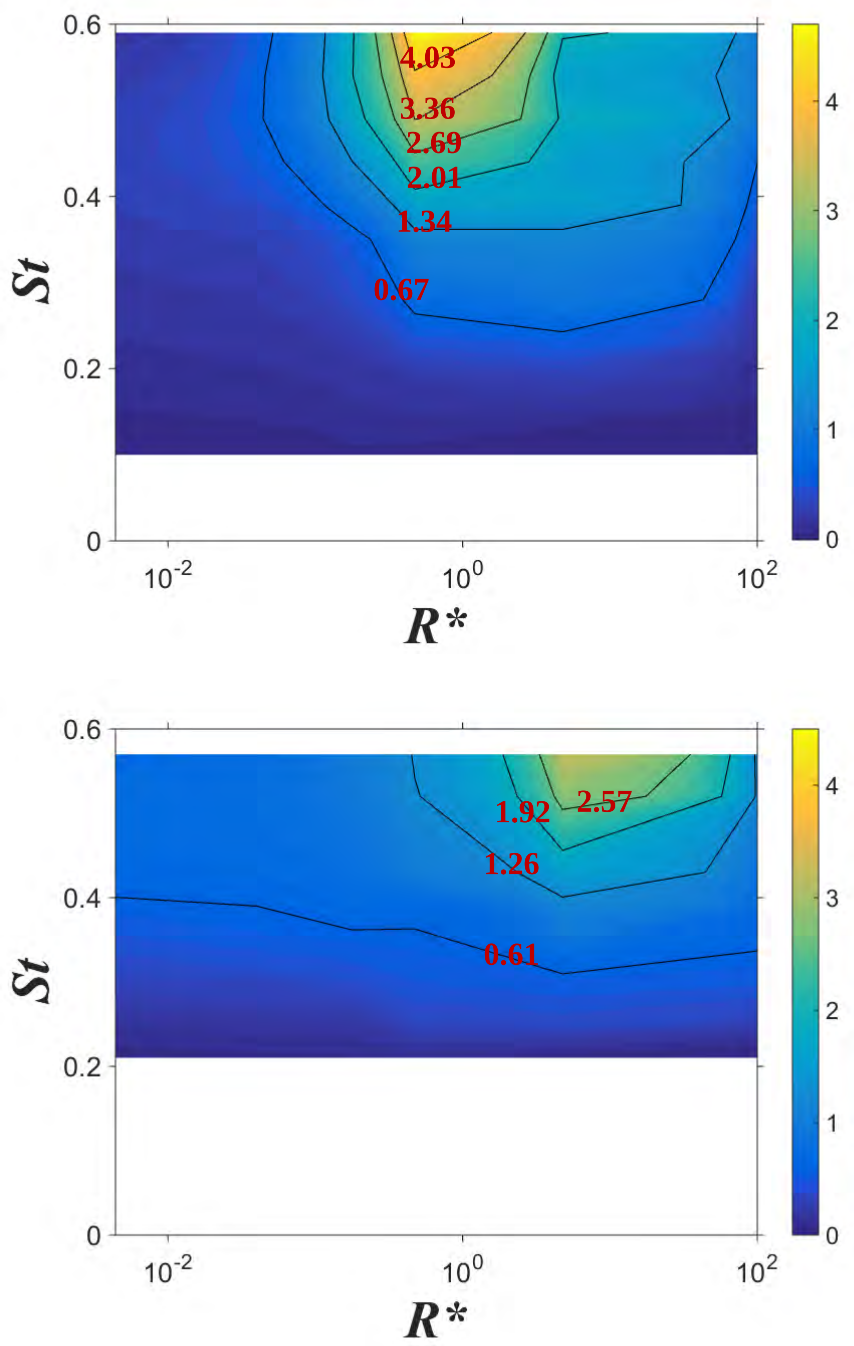

Figure 3.14. Contour plot showing the variation of C_T for (a) $h_0/c = 0.11$ and (b) $h_0/c = 0.32$

3.4.3 Power coefficient

Power coefficient is always increasing with Strouhal number for both $h_0/c = 0.11$ and 0.32. In case of $h_0/c = 0.11$ power coefficient is initially increasing, attaining its maxima at 0.473 and again decreases. While in the other case i.e. $h_0/c = 0.32$, maximum value of C_P is corresponding to St = 4.73.

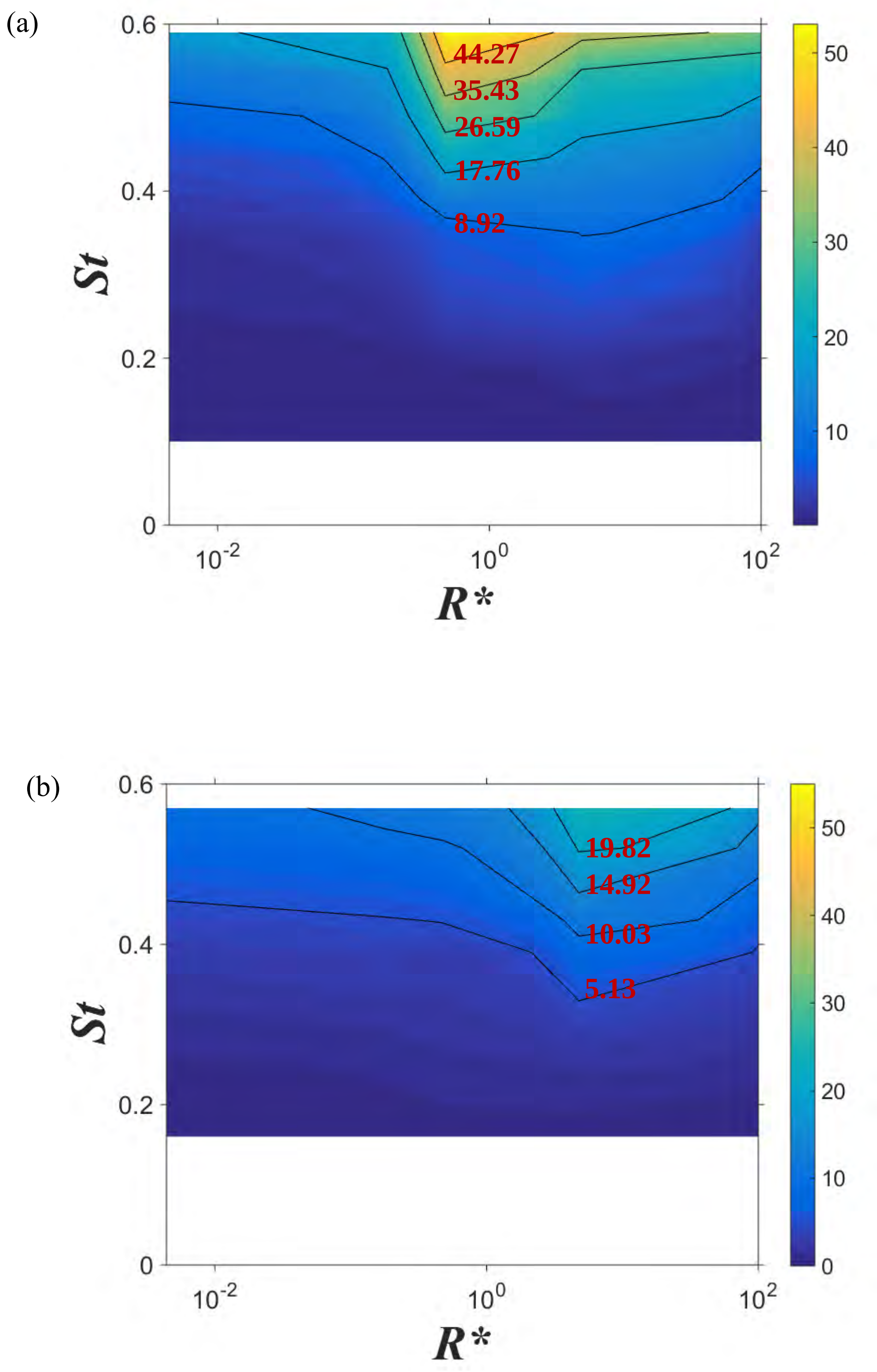

Figure 3.15. Contour plot showing the variation of C_P for (a) $h_0/c = 0.11$ and (b) $h_0/c = 0.32$

3.5 Summary

Results obtained in the present work can be summarized as:

h_0/c	R*	EI (Nm)	η_{max} (%)	Quantities corresponding to η_{max}			
				St	C_T	C_P	$\frac{\eta}{\eta_{rigid}}$
0.11	0.0044	5.77 X 10^{-6}	30.27	0.19	0.12	0.39	1.66
	0.177	2.34 X 10^{-4}	34.95	0.13	0.09	0.27	1.91
	0.473	**6.27 X 10^{-4}**	**35.17**	**0.16**	**0.17**	**0.47**	**1.92**
	4.73	6.32 X 10^{-3}	18.66	0.19	0.30	1.62	1.02
	Rigid	-	18.29	0.13	0.04	0.22	1
0.32	0.0044	5.77 X 10^{-6}	24.06	0.30	0.33	1.37	0.95
	0.177	2.34 X 10^{-4}	22.84	0.30	0.42	1.83	0.90
	0.473	6.27 X 10^{-4}	24.64	0.25	0.35	1.42	0.97
	4.73	6.32 X 10^{-3}	19.52	0.25	0.38	1.97	0.77
	Rigid	**-**	**25.43**	**0.30**	**0.51**	**2.02**	**1**

Table 3.2. Result summary of present work on heaving foil at h_0/c 0.11 and 0.32.

The overall maximum efficiency (η) attained is 35.17 % at h_0/c = 0.11, St = 0.16 and R* = 0.473. Corresponding values of thrust coefficient (C_T) and power coefficient (C_P) are 0.17 and 0.47 respectively. Though efficiencies are higher for lower heave amplitude, but the corresponding thrust coefficients are much lower in comparison to higher heave amplitude.

Similar work has been done on pure pitching oscillation with pitch amplitude, $\theta_0 = 15^0$ in sinusoidal waveform by Sunil in our lab. He obtained the overall maximum efficiency (η) of 45 % at R* = 0.012 and St = 0.25. Corresponding values of thrust coefficient (C_T) and power coefficient (C_P) are 0.5 and 1.11 respectively.

θ_0	R*	EI (Nm)	η_{max} (%)	Quantities corresponding to η_{max}			
				St	C_T	C_P	$\frac{\eta}{\eta_{rigid}}$
15^0	**0.012**	**6.78 X 10^{-5}**	**45**	**0.25**	**0.5**	**1.11**	**3.75**
	0.2	2.86 X 10^{-3}	32	0.32	1.0	3.12	2.67
	8.203	2.86 X 10^{-3}	24	0.35	2.0	8.33	2
	18	1.09 X 10^{-2}	18	0.30	1.5	8.33	1.5
	Rigid	-	12	0.35	0.2	1.67	1

Table 3.3. Result summary on pitching foil at $\theta_0 = 15^0$ done by Sunil.

4 Conclusion

In the present study, we have experimentally investigated propulsive parameters of heaving foils. The study comprises of effect of variation of heave amplitudes and effect of chord-wise flexibility. The mean thrust generated (C_T) and propulsive efficiency (η) are both obtained experimentally from force and moment measurements using load cell.

All the parameters have been studied as a function of Strouhal number (St). Mean thrust generated (C_T) and mean power coefficient (C_P) has not increased much with increase in heave amplitude at same Strouhal number (St) as heave amplitude is already accommodated in St. Maximum efficiency increases with heave amplitude for rigid foil. But for flexible case it is lower for higher heave amplitude.

The overall maximum efficiency obtained is 35.2 % for $h_0/c = 0.11$ at St = 0.16 and R* = 0.473, but the corresponding C_T is 0.167 which is significantly low. For the larger heave amplitude case of $h_0/c = 0.32$, the maximum efficiency attained is 25.43 % at St = 0.3 for rigid foil with corresponding $C_T = 0.51$.

5 Future work

- As an extension of current work, there can be wake studies through PIV of specific cases where we have obtained maximum propulsive efficiency, for better understanding of physics behind such propulsive behaviours.
- Optimization of h_0/c can be done, by studying a more wider range of the parameter.
- There can be variation on the texture of foil to mimic fish skins and studying their effects on propulsive characteristics.
- Combination of heave and pitch oscillation with desired phase difference can be studied.
- Furthermore, there is an increasing evidence that fish gain energetic benefits from the hydrodynamic interactions when they swim in a school. To study this effect of schooling on propulsive parameters, foils can be oscillated side by side or one down stream of other.

6 Appendix

In the present work, experiments have been performed with heaving foil with different flexural rigidity. Results of rigid foil and flexible foil with R* = 0.0044 and 0.473 have already been shown. Additionally, flexible foil with R* = 0.0177 and 4.73 have also been studied.

6.1 R* = 0.177

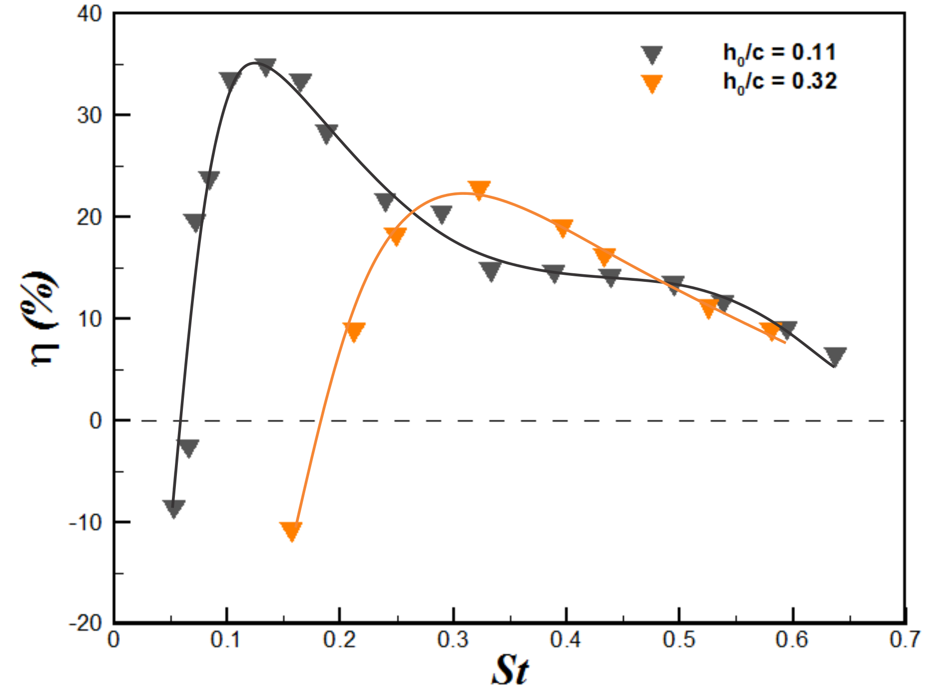

Figure 6.1. R* = 0.177. Efficiency is plotted as a function of Strouhal number, St for heaving foil with $h_0/c = 0.11$, $h_0/c = 0.32$.

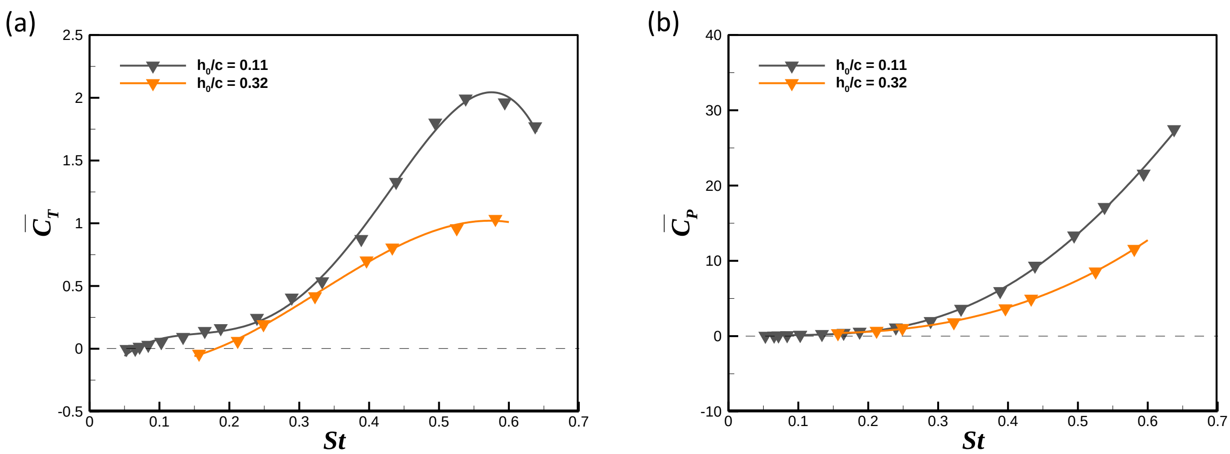

Figure 6.2. R* = 0.177. (a) Mean thrust coefficient, $\overline{C_T}$ and (b) power coefficient, $\overline{C_P}$ as a function of St for h_0/c =0.11 and 0.32

6.2 R* = 4.73

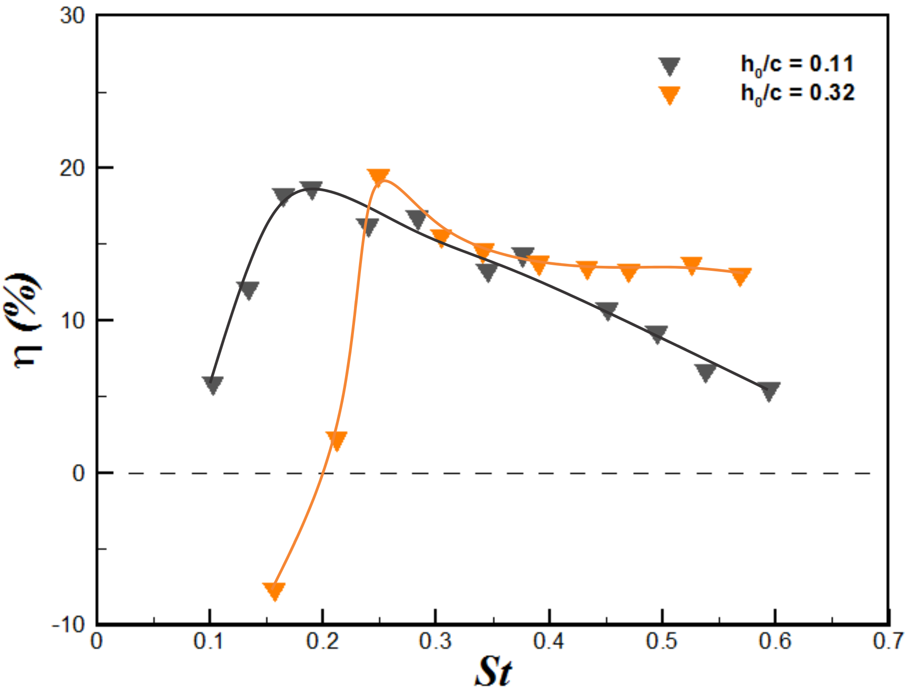

Figure 6.3. R* = 4.73. Efficiency is plotted as a function Strouhal number, St for heaving foil with h_0/c = 0.11, h_0/c = 0.32.

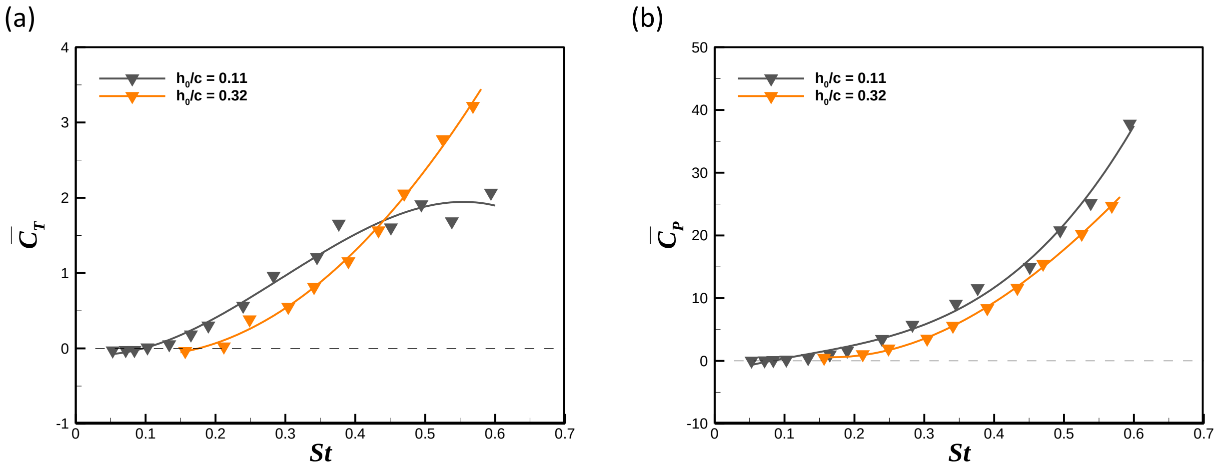

Figure 6.4. R* = 4.73. (a) Mean thrust coefficient, $\overline{C_T}$ and (b) power coefficient, $\overline{C_P}$ as a function of St for h_0/c =0.11 and 0.32

References

1) Garrick, I. E. 1936 Propulsion of a flapping and oscillating airfoil. NACA Tech. Rep. 567.
2) De Laurier, J. D.& Harris, J. M. 1982 Experimental study of oscillating wing propulsion. J. Aircraft 19 (5), 368-373.
3) Freymuth, P. 1988 Propulsive vortical signature of plunging and pitching airfoils. AIAA J. 26, 881-883.
4) A. W. Mackowski and C. H. K. Williamson. 2017 Effect of pivot location and passive heave on propulsion from a pitching airfoil.
5) J. M. Anderson, K. Streitlien, D. S. Barrett, and M. S. Triantafyllou, Oscillating foils of high propulsive efficiency, J. Fluid Mech. 360, 41 (1998).
6) D. A. Read, F. S.Hover, andM. S. Triantafyllou, Forces on oscillating foils for propulsion and maneuvering, J. Fluids Struct. 17, 163 (2003).
7) Journal of the Indian Institute of Science VOL 91:3 July–Sept. 2011.
8) Lindsey C.C., 1978 Form, Function and Locomotory Habits in Fish.
9) J. M. Miao and M. H. Ho, Effect of flexure on aerodynamic propulsive efficiency of flapping flexible airfoil, J. Fluids Struct. 22, 401 (2006).
10) Alexander J. Smits et al. 2017, Non-sinusoidal gaits for unsteady propulsion.
11) M. Jimreeves David et al. Thrust generation from pitching foils withflexible trailing edge flaps, J. Fluid Mech. (2017).